



HAL
open science

Consideration of soil types for the calibration of molecular proxies for soil pH and temperature using global soil datasets and Vietnamese soil profiles

Nina Davtian, Guillemette Ménot, Edouard Bard, Jérôme Poulénard, Pascal Podwojewski

► To cite this version:

Nina Davtian, Guillemette Ménot, Edouard Bard, Jérôme Poulénard, Pascal Podwojewski. Consideration of soil types for the calibration of molecular proxies for soil pH and temperature using global soil datasets and Vietnamese soil profiles. *Organic Geochemistry*, 2016, 101, pp.140 - 153. 10.1016/j.orggeochem.2016.09.002 . hal-01683011

HAL Id: hal-01683011

<https://hal.science/hal-01683011>

Submitted on 2 Feb 2024

HAL is a multi-disciplinary open access archive for the deposit and dissemination of scientific research documents, whether they are published or not. The documents may come from teaching and research institutions in France or abroad, or from public or private research centers.

L'archive ouverte pluridisciplinaire **HAL**, est destinée au dépôt et à la diffusion de documents scientifiques de niveau recherche, publiés ou non, émanant des établissements d'enseignement et de recherche français ou étrangers, des laboratoires publics ou privés.

1 Consideration of soil types for the calibration of molecular
2 proxies for soil pH and temperature using global soil datasets
3 and Vietnamese soil profiles

4

5 Nina Davtian ^{a,*}, Guillemette Ménot ^b, Edouard Bard ^a, Jérôme Poulénard ^c,
6 Pascal Podwojewski ^{d,e}

7

8 ^a *Aix-Marseille Université, CNRS, IRD, Collège de France, CEREGE UM34,*
9 *Aix-en-Provence 13545, France*

10 ^b *Laboratoire de Géologie de Lyon, Terre, Planètes, Environnement, CNRS*
11 *UMR 5276, Ecole Normale Supérieure de Lyon, Université Claude Bernard*
12 *Lyon 1, France*

13 ^c *EDYTEM, Université de Savoie/CNRS, 73376 Le Bourget du Lac, France*

14 ^d *IRD, UMR 242 IEES-Paris, 32 avenue Henri Varagnat, 93143 Bondy cedex,*
15 *France*

16 ^e *IRD, UMR 242 IEES-Paris, School of Agriculture, Earth and*
17 *Environmental Science, University of KwaZulu-Natal, Box X01, Scottsville,*
18 *3209, South Africa*

19

20 *Corresponding author. *E-mail address:* davtian@cerege.fr (N. Davtian)

22 **ABSTRACT**

23 Distribution of branched glycerol dialkyl glycerol tetraethers (brGDGTs) in
24 soils depends on environmental parameters such as mean annual air
25 temperature (MAAT) and soil pH. MBT'/MBT'_{5ME} (methylation index of
26 branched tetraethers) and CBT/CBT' (cyclization ratio of branched
27 tetraethers) are ratios based on the relative abundances of brGDGTs. Using
28 these ratios, global and regional/local calibrations have been established
29 using surface soils, but generally without any preliminary study of soil
30 types. In this study, we reconsider global MAAT–pH/brGDGT calibrations
31 by assigning soil types to the 358 components of a composite soil dataset.
32 Additionally, we investigate brGDGT-derived proxies in five well-described
33 soil profiles along an altitudinal transect in the Mount Fan Si Pan National
34 Park, northwestern Vietnam. Our results show that at the global scale,
35 traditional MAAT–pH/brGDGT relationships per soil type are significantly
36 different and that MAAT(pH) residuals per soil type may differ as well, for
37 example between Alisols and Podzols. This effect persists when 5- and 6-
38 methyl brGDGTs are quantified separately. In addition, MAAT(pH)
39 residuals per soil type are generally not clearly reduced, including in
40 Leptosols, in which 6-methyl brGDGTs are present. In the Fan Si Pan
41 transect, MBT'/CBT' –MAAT estimates showed no significant deviation from
42 expected MAATs. We find, however, that soil type effect – related to
43 vegetation changes and contrasting soil organic carbon properties – may
44 bias MAAT–pH estimates in the Vietnamese soil transect. Additionally, soil

45 depth plays a role which differs between the different Fan Si Pan soil
46 profiles, likely determined by soil type and history.

47

48 *Keywords:* calibration, soil, brGDGTs, temperature, pH

49

50 1. Introduction

51 Branched glycerol dialkyl glycerol tetraethers (brGDGTs) are
52 membrane lipids of high molecular weight (Fig. 1) that are of bacterial
53 origin (Weijers et al., 2006a, 2009; Sinninghe Damsté et al., 2011, 2014).
54 They are ubiquitous in aquatic and continental environments (Schouten et
55 al., 2013 and references therein). At the global scale, brGDGT distributions
56 in soils mainly depend on mean annual air temperature (MAAT) and soil pH
57 (e.g., Weijers et al., 2007; Peterse et al., 2012). Several indices have been
58 developed to summarize brGDGT distributions, for instance the methylation
59 index of branched tetraethers (MBT), the cyclization ratio of branched
60 tetraethers (CBT) and the MBT' index, which is a simplified form of MBT.
61 These indices are linked to continental temperatures and soil pH through
62 two global soil calibrations. However, calibration errors are about 5.0 °C and
63 about 0.8 pH unit (Weijers et al., 2007; Peterse et al., 2012). High
64 calibration errors are due to multiple possible biases such as soil texture,
65 humidity and oxygenation (e.g. Peterse et al., 2009a; Huguet et al., 2010;
66 Dirghangi et al., 2013; Menges et al., 2014; Dang et al., 2016), seasonality
67 and/or use of atmospheric rather than soil temperature (e.g., Peterse et al.,
68 2012; Deng et al., 2016; Wang et al., 2016). Indeed, MAAT is an
69 approximation of mean annual soil temperature that is also influenced by
70 other climate-dependent parameters, such as snow cover, vegetation type
71 and soil properties (Smerdon et al., 2004). Recently, new indices such as
72 MBT'_{5ME}, CBT'_{5ME} and CBT' have been defined, following analytical

73 improvements that have allowed the separate quantification of 5- and 6-
74 methyl brGDGTs (Fig. 1; De Jonge et al., 2014). Poor brGDGT separations
75 also explain part of the scatter in the global calibrations (De Jonge et al.,
76 2014).

77 As also seen at the global scale, substantial scatter has been observed
78 at the regional/local scale, including for calibrations based on altitudinal
79 transects (Sinninghe Damsté et al., 2008; Peterse et al., 2009b; Yang et al.,
80 2010, 2015b; Ernst et al., 2013; Liu et al., 2013; Anderson et al., 2014;
81 Coffinet et al., 2014; Zhuang et al., 2015; Deng et al., 2016; Nieto-Moreno et
82 al., 2016). Factors other than MAAT and pH, such as vegetation and soil
83 type, length of growing season and topography, have been suggested as
84 causes for part of the scatter (Sinninghe Damsté et al., 2008; Peterse et al.,
85 2009b; Liu et al., 2013; Anderson et al., 2014; Deng et al., 2016; Nieto-
86 Moreno et al., 2016). Contrary to the classical MBT' index, MBT'_{5ME} is well
87 correlated with MAAT/altitude at Mt. Shennongjia, China (Yang et al.,
88 2015a, 2015b). It is noteworthy that only a few previous brGDGT-based
89 studies have used well-described soils and/or profiles (Huguet et al., 2010;
90 Zech et al., 2012; Menges et al., 2014; Yamamoto et al., 2016). A better
91 consideration of soil pedogenesis may help researchers to properly evaluate
92 the dependency of the observed scatters on soil physico-chemical properties.

93 In the present study, we reassess a composite global soil dataset
94 (Huguet et al., 2010; Peterse et al., 2012; Dirghangi et al., 2013; Anderson et
95 al., 2014; De Jonge et al., 2014) by assigning a soil type to each of its 358

96 components to investigate traditional and newest MAAT–pH/brGDGT
97 relationships as well as MAAT(pH) residuals, per soil type. We also take
98 advantage of a well-characterized altitudinal soil transect with an elevation
99 range of 1400 m in the Mount Fan Si Pan National Park, Vietnam
100 (Podwojewski et al., 2011) to investigate brGDGT distributions. We focus, in
101 particular, on the possible vegetation/soil type and depth effect and assess
102 how well brGDGT-derived proxies reflect MAAT and soil pH in Vietnam.

103

104 **2. Materials and methods**

105 *2.1. Soil type assignment for the global soil dataset and statistical analysis*

106 A composite global soil dataset of 358 previously analyzed samples
107 (Supplementary Table S1; Huguet et al., 2010; Peterse et al., 2012;
108 Dirghangi et al., 2013; Anderson et al., 2014; De Jonge et al., 2014) was
109 used for soil type assignment. For most samples taken from the
110 International Soil Reference and Information Centre (ISRIC), soil types
111 were obtained using the ISRIC Soil Information System (ISIS) database
112 (<http://isis.isric.nl>, last accessed on Thursday, August 25, 2016). For the
113 other samples, with the exception of those analyzed by Huguet et al. (2010)
114 which were the subject of preliminary pedological studies, the most likely
115 soil type was selected using the SoilInfo App based on SoilGrids1km (Hengl
116 et al., 2014; <https://soilinfo-app.org>, version 0.5.0, 15 November, 2015,
117 accessed before the update to SoilGrids250m in June 2016).

118 Statistical analysis – correlation tests, linear regressions and
 119 homogeneity of slopes test/analysis of covariance (ANCOVA) – was
 120 conducted using the statistical software R 3.1.2 (R Development Core Team,
 121 2016). Prior to the investigation of each MAAT–brGDGT and each pH–
 122 brGDGT relationship, the outliers were eliminated using the car package
 123 (Fox and Weisberg, 2011). After conducting repeated outlier tests until no
 124 more samples with a Bonferroni p -value < 0.05 remained, all the identified
 125 outliers were excluded from further statistical analysis. The slope
 126 homogeneity test was then conducted to verify whether regression slopes
 127 per soil type for a given MAAT–brGDGT or pH–brGDGT relationship were
 128 statistically identical – the ANCOVA being conducted only when the
 129 homogeneity of slopes test was not significant, i.e. p -value ≥ 0.05 . Only soil
 130 types with at least 10 samples after exclusion of outliers and samples with
 131 missing data were selected for statistical analysis.

132 All MAAT–pH residuals in this study were determined using the
 133 global soil calibrations of Peterse et al. (2012) following equations (1) and
 134 (2), and of De Jonge et al. (2014) following equations (3) and (4):

$$\text{MAAT} = 0.81 - 5.67 \times \text{CBT} + 31.00 \times \text{MBT}' \quad (1)$$

$$\text{pH} = 7.90 - 1.97 \times \text{CBT} \quad (2)$$

$$\text{MAAT} = - 8.57 + 31.45 \times \text{MBT}'_{5\text{ME}} \quad (3)$$

$$\text{pH} = 7.15 + 1.59 \times \text{CBT}' \quad (4)$$

135 With MBT', CBT, MBT'_{5ME} and CBT' defined as follows:

$$\text{MBT}' = \frac{\text{Ia} + \text{Ib} + \text{Ic}}{\text{Ia} + \text{Ib} + \text{Ic} + \text{IIa} + \text{IIb} + \text{IIc} + \text{IIIa} + \text{IIa}' + \text{IIb}' + \text{IIc}' + \text{IIIa}'} \quad (5)$$

$$\text{CBT} = -\log\left(\frac{\text{Ib} + \text{IIb} + \text{IIb}'}{\text{Ia} + \text{IIa} + \text{IIa}'}\right) \quad (6)$$

$$\text{MBT}'_{5\text{ME}} = \frac{\text{Ia} + \text{Ib} + \text{Ic}}{\text{Ia} + \text{Ib} + \text{Ic} + \text{IIa} + \text{IIb} + \text{IIc} + \text{IIIa}} \quad (7)$$

$$\text{CBT}' = \log\left(\frac{\text{Ic} + \text{IIa}' + \text{IIb}' + \text{IIc}' + \text{IIIa}' + \text{IIIb}' + \text{IIIc}'}{\text{Ia} + \text{IIa} + \text{IIIa}}\right) \quad (8)$$

136 Roman numerals refer to the structures in Fig. 1.

137 Prior to any residual per soil type inspection, Z-scores and Tukey box
 138 plots were used to eliminate all outliers. Once again, only soil types with at
 139 least 10 samples after elimination of outliers and samples with missing data
 140 were considered.

141

142 2.2. *Environmental setting in the Mount Fan Si Pan National Park and* 143 *MAAT modeling*

144 The environmental setting is described in detail by Podwojewski et al.
 145 (2011). In short, the Mount Fan Si Pan National Park (22°18'13"3N,
 146 103°46'32"5E) is located in northwestern Vietnam, close to the Chinese
 147 border (Fig. 2A). The Fan Si Pan Mountain range is oriented northwest–
 148 southeast and culminates at 3143 m above modern sea level, the highest
 149 altitude in Vietnam (Podwojewski et al., 2011). The soil bedrock is
 150 homogenous throughout the entire mountain range and the anthropic
 151 influences are restricted to the foothills, the rest of the mountain range
 152 being covered with primary C₃ vegetation that follows a pronounced
 153 altitudinal zonation (Fig. 2B; Podwojewski et al., 2011). The Mount Fan Si
 154 Pan National Park is subject to a typical monsoonal climate, albeit altered

155 by altitude and orientation to the winds as air moisture is high all year
156 round with frequent drizzle and fog (Podwojewski et al., 2011).

157 A linear ordinary least square regression of MAAT vs altitude was
158 established using MAAT data as y values from 17 weather stations in
159 Vietnam and China (Supplementary Table S2) in addition to the Hoang
160 Lien Son Mountain MAAT value as reported in Podwojewski et al. (2011).
161 The obtained slope and intercept were -4.5 ± 0.2 °C/km and 23.2 ± 0.2 °C,
162 the 1- σ root mean square error (RMSE) was 0.6 °C and the *p*-value was
163 much lower than 0.001. The established linear regression was then applied
164 to the Mount Fan Si Pan National Park to derive MAAT at any altitude.

165

166 2.3. *Fan Si Pan soil profiles and samples*

167 The pedological study of Podwojewski et al. (2011) represented an
168 opportunity to couple brGDGT distributions to soil types, as the latter had
169 already been reliably determined. Ten soil pits had previously been
170 excavated along the Fan Si Pan Mountain by Podwojewski et al. (2011). The
171 soils were initially sampled for soil type characterization – soil organic
172 matter properties and geochemical environment – with respect to
173 environmental changes. Five of the initially investigated soil profiles were
174 selected for this study (FAN 1, FAN 2 and FAN 4 to FAN 6; Fig. 2) as they
175 occur along a well-defined transect (Fig. 2A) and cover the entire
176 pedogenetic sequence (Fig. 2B; Podwojewski et al., 2011). The selected soil
177 profiles and horizons are described in detail by Podwojewski et al. (2011). In

178 short, Podwojewski et al. (2011) described shallow (< 1 m deep) and very
179 acidic soils (3.5–4.7 pH units, measured with a 1:2.5 soil:water ratio) with
180 variable bulk organic carbon (C_{org}) concentrations (0.4–44.1%) and high
181 water content values (40–215%). $\delta^{13}C$ analyses enabled Podwojewski et al.
182 (2011) to confirm C_{org} inputs from dominant C_3 vegetation at every altitude.
183 Podwojewski et al. (2011) also made a floristic inventory at each soil
184 sampling site (Fig. 2B) and distinguished three main climate/vegetation-
185 dependent soil types:

- 186 (i) Low altitude Acrisols/Alisols – strongly weathered acidic soils with
187 low base saturation at some depth, typical under warm and wet
188 conditions (Podwojewski et al., 2011 and references therein; IUSS
189 Working Group WRB, 2015) – represented by FAN 1 and FAN 2.
- 190 (ii) Mid-altitude Podzols – acidic soils with an organic layer and an
191 ash-looking eluvial horizon directly underlain by the illuvial *spodic*
192 or Bs horizon due to the accumulation of organo-metallic (Fe, Al)
193 complexes leached by rainwater, typical in cold/temperate forests
194 and in tropical mountain forests (Podwojewski et al., 2011 and
195 references therein; IUSS Working Group WRB, 2015) –
196 represented by FAN 4 and FAN 5.
- 197 (iii) High altitude Umbrisols – soils with dark topsoil, thick, well-
198 humified and desaturated in the Mount Fan Si Pan National Park,
199 typical under humid conditions with little or no moisture deficit in
200 cool/temperate areas and in (sub)tropical mountain shrub and

201 grasslands (Podwojewski et al., 2011 and references therein; IUSS
202 Working Group WRB, 2015) – represented by FAN 6.

203

204 2.4. Sample preparation and *brGDGT* analysis

205 The samples were air dried and sieved through a 2 mm sieve before
206 being ground and homogenized using a mortar and pestle. Between 0.8 and
207 2.2 g of each sample, depending on C_{org} concentration, was then extracted
208 with DCM:MeOH (9:1, v:v) using an accelerated solvent extractor ASE 350
209 Dionex at 120 °C and 10^7 Pa. Total lipid extracts were separated following
210 the automated procedure established by Sanchi et al. (2013).

211 BrGDGT analyses were performed at CEREGE by high-performance
212 liquid chromatography–atmospheric pressure chemical ionization mass
213 spectrometry (HPLC–APCI-MS) using positive ions on a HPLC–MS 1100
214 Series spectrometer, following Sanchi et al. (2014).

215 The MBT' and CBT indices were calculated using equations (5) and
216 (6). Since no local/regional calibration has yet been established for Vietnam,
217 MAAT and pH were estimated using the extended global soil calibration
218 developed by Peterse et al. (2012), equations (1) and (2).

219 The BIT index was calculated following Hopmans et al. (2004):

$$\text{BIT} = \frac{\text{Ia} + \text{IIa} + \text{IIIa} + \text{IIa}' + \text{IIIa}'}{\text{Cren} + \text{Ia} + \text{IIa} + \text{IIIa} + \text{IIa}' + \text{IIIa}'} \quad (9)$$

220 Roman numerals refer to the structures in Fig. 1.

221 Based on duplicate injections of the entire sample set, the mean
222 analytical 1- σ standard deviations (SD, mean of 1- σ SD to individual mean

223 values) were 0.003 for MBT', 0.006 for CBT and 0.001 for BIT. These
224 correspond to 0.1 °C and 0.01 pH unit mean analytical uncertainties.

225

226 **3. Results**

227 *3.1. Global MAAT–pH/brGDGT relationships and MAAT–pH residuals* 228 *per soil type*

229 Twenty-seven different soil types were represented in the 358-
230 component composite global soil dataset (Fig. 3). Visually, the scatters per
231 soil type were not all similar and some soil types such as Luvisols and
232 Regosols were mainly clustered into relatively small MAAT–pH/brGDGT
233 domains and/or comprised a few outliers (Fig. 3 and Supplementary Fig.
234 S1). The composite dataset allowed us to extend the number of soil types
235 suitable for statistical analysis from eight to twelve – from 174 to 298 soil
236 samples. MAAT–pH/brGDGT relationships (Tables 1 and 2) and MAAT(pH)
237 residual distributions (Fig. 4) were thus determined for the most
238 represented soil types only. A few examples of soil types were also selected
239 for more detailed MAAT residual distributions (Fig. 5). The soil samples
240 reconsidered by De Jonge et al. (2014) were used to compare the newest
241 with traditional MAAT–pH/brGDGT relationships per soil type, as well as
242 MAAT(pH) residual distributions per soil type using traditional and newest
243 global soil calibrations (Figs. 4 and 5, Table 2).

244 Using the composite global soil dataset, five soil types had non-
245 significant MAAT–MBT'/CBT relationships and seven soil types had non-

246 significant pH–CBT relationships (Table 1). For MAAT–MBT'/CBT, the R^2
247 range was 0.0–0.8 and the RMSE range was 2.2–7.0 °C. For pH–CBT, the R^2
248 range was 0.0–0.8 and the RMSE range was 0.4–1.0 pH units (Table 1).
249 Ranges of MAAT–MBT'/CBT coefficients were 46.9 for MBT' slope, 11.7 for
250 CBT slope and 24.7 for intercept (Table 1). Some pairs of soil types, – for
251 example Andosols and Cambisols – had similar coefficients whereas other
252 pairs of soil types such as Cambisols and Luvisols had at least one
253 coefficient that was significantly different (Table 1). Ranges of pH–CBT
254 coefficients were 2.4 for slope and 3.4 for intercept (Table 1). After the
255 homogeneity of slopes test ($F = 4.83$, $p < 0.001$), pH–CBT slopes per soil type
256 were not all similar. For instance, they were similar between Cambisols and
257 Leptosols, but not between Cambisols and Luvisols (Table 1). When
258 compared to the global MAAT–pH/brGDGT relationships, three soil types
259 had similar MAAT–MBT'/CBT coefficients and three soil types had similar
260 pH–CBT coefficients (Table 1).

261 Using the global soil dataset of De Jonge et al. (2014), two or three
262 soil types had non-significant traditional and new MAAT–pH/brGDGT
263 relationships (Table 2). For MAAT–MBT'/CBT vs MAAT–MBT'_{5ME}, the R^2
264 range was 0.1–0.9 vs 0.0–0.9 and the RMSE range was 1.6–6.8 °C vs 2.4–5.6
265 °C. For pH–CBT vs pH–CBT', the R^2 range was 0.1–0.7 vs 0.0–0.9 and the
266 RMSE range was 0.5–1.1 pH units vs 0.2–0.6 pH units (Table 2). Ranges of
267 MAAT–MBT'/CBT coefficients were 60.6 for MBT' slope, 10.9 for CBT slope
268 and 22.2 for intercept whereas ranges of MAAT–MBT'_{5ME} coefficients were

269 46.2 for slope and 34.2 for intercept (Table 2). Ranges of pH–CBT vs pH-
270 CBT' coefficients were 1.9 vs 1.8 for slope and 3.0 vs 2.8 for intercept (Table
271 2). For all bivariate traditional and newest MAAT–pH/brGDGT
272 relationships, slopes/intercepts per soil type were not all similar after the
273 homogeneity of slopes tests/ANCOVA (Table 2). When compared to the
274 global MAAT–brGDGT relationships, four soil types had similar MAAT–
275 MBT'/CBT coefficients and six soil types had similar MAAT–MBT'_{5ME}
276 coefficients (Table 2). When compared to the global pH–brGDGT
277 relationships, three soil types had similar pH–CBT coefficients and two soil
278 types had similar pH–CBT' coefficients (Table 2).

279 Using the composite global soil dataset, mean MAAT residuals per
280 soil type based on the MAAT–MBT'/CBT global soil calibration of Peterse et
281 al. (2012) varied between –7.0 and 3.5 °C (Figs. 4A, 5A and 5B). Mean pH
282 residuals per soil type based on the pH–CBT global soil calibration of
283 Peterse et al. (2012) varied between –1.3 and 0.4 pH units (data not shown).

284 Using the global soil dataset of De Jonge et al. (2014), mean MAAT
285 residuals per soil type based on the MAAT–MBT'/CBT global soil calibration
286 of Peterse et al. (2012) varied between –7.5 and 3.5 °C (Figs. 4B, 5C and 5E).
287 Mean MAAT residuals per soil type based on the MAAT–MBT'_{5ME} global soil
288 calibration of De Jonge et al. (2014) varied between –3.5 and 2.5 °C (Figs.
289 4C, 5D and 5F). Mean pH residuals per soil type based on the pH–CBT
290 global soil calibration of Peterse et al. (2012) varied between –1.4 and 0.2
291 pH units (data not shown). Mean pH residuals per soil type based on the

292 pH–CBT' global soil calibration of De Jonge et al. (2014) varied between –0.2
293 and 0.3 pH units (data not shown).

294

295 3.2. *BrGDGT distributions and proxies in the Fan Si Pan National Park*

296 BrGDGTs were present in all Fan Si Pan soil samples. Compounds Ia
297 and IIa/IIa' were the most abundant in each sample, representing together
298 at least 86% of total brGDGTs (Supplementary Table S3). Conversely,
299 compounds IIIb/IIIb' and IIIc/IIIc' were all reliably detected in only one-
300 third of the samples, precluding the use of MBT and associated soil
301 calibrations.

302 BIT, MBT' and CBT were calculated for all Fan Si Pan soil samples
303 (Fig. 6, Table 3). The BIT range was 0.94–1.00, the MBT' range was 0.57–
304 0.93 and the CBT range was 1.02–2.01 (Table 3). The MBT'/CBT-based
305 MAAT estimate range was 10.0–20.5 °C using the global soil calibration of
306 Peterse et al. (2012), corresponding to differences with modeled MAAT
307 between –2.8 and 6.2 °C – on average 2.3 ± 1.7 °C (Table 3). The CBT-based
308 pH estimate range was 3.9–5.9 pH units using the global soil calibration of
309 Peterse et al. (2012), corresponding to differences with measured pH
310 between –0.1 and 2.1 pH units – on average 0.9 ± 0.6 pH units (Table 3).

311 BIT varied with depth by maximum 0.04 in all soil profiles (Fig. 6).
312 MBT' decreased with depth by 0.14–0.21 in Podzols (even if FAN 5 had only
313 three points), looked globally stable in FAN 1 (also with only three points),
314 and was stable in the other soil profiles. CBT was stable in FAN 5,

315 fluctuated by 0.25–0.50 in FAN 6, and decreased with depth by 0.24–0.66 in
316 the other soil profiles. CBT-based pH variations with depth were opposite
317 and roughly twice as high as CBT variations with depth in all soil profiles.
318 Measured pH increased with depth by 0.5–1.3 pH units in all soil profiles,
319 except FAN 5 with only two points (Fig. 6). However, in FAN 4 and FAN 6,
320 changes in measured pH with depth shifted from decreases in A horizons to
321 increases in B horizons, with variations of 0.2–0.6 pH units in FAN 6 and of
322 0.4–1.0 pH units in FAN 4. MBT/CBT-based MAAT decreased with depth
323 by about 4–6 °C in Podzols, increased by about 2.5 °C in Acrisols/Alisols, and
324 was stable in Umbrisols (Fig. 6).

325

326 4. Discussion

327 4.1. Global soil dataset

328 4.1.1. Soil type diversity and implications for MAAT–pH reconstructions

329 The 27 soil types represented in the 358-component composite global
330 soil dataset denote its high diversity (Fig. 3 and Supplementary Fig. S1,
331 Supplementary Table S1). Most of the soil samples were taken from surficial
332 and/or A horizons (Supplementary Table S1). Thus, we may assume that soil
333 depth has no significant effect on the global brGDGT distributions
334 considered in this study.

335 Pedogenetic processes depend on multiple factors such as climate,
336 vegetation type, topography and parent material (e.g., IUSS Working Group
337 WRB, 2015). These differential processes in soil formation and erosion may

338 have an impact on the production, transformation and preservation of labile
339 substrates for brGDGT producers, including in surficial horizons. Indeed,
340 brGDGT producers are partially attributable to *Acidobacteria* (Weijers et
341 al., 2009; Sinninghe Damsté et al., 2011, 2014) and their metabolism is
342 thought to be the heterotrophic assimilation of labile substrates or the
343 chemoautotrophic consumption of respired CO₂ (Weijers et al., 2010).

344 Given the specificity of soil types to climatic ranges such as moisture
345 regime/mean annual precipitation (MAP, Fig. 4, Supplementary Table S1),
346 some soil types have small MAAT and/or pH domains that may be
347 associated with small MBT' and/or CBT domains, which may result in non-
348 significant MAAT–pH/brGDGT relationships (Fig. 3, Table 1 and
349 Supplementary Table S1). For instance, Acrisols, Alisols, Ferralsols, Podzols
350 and Umbrisols did not show a significant pH–CBT anti-correlation, likely
351 due to their typically low pH values and high CBT values (Table 1 and
352 Supplementary S1). Alisols and Ferralsols also had typically high MAAT
353 and MBT' values, resulting in non-significant MAAT–MBT'/CBT
354 relationships (Table 1 and Supplementary Table S1).

355 Regression coefficients and performances of MAAT–MBT'/CBT and
356 pH–CBT differed at times between different soil types, whose MAAT–
357 pH/brGDGT relationships were not always similar to global ones (Table 1).
358 After the homogeneity of slopes test, at least one soil type had a
359 significantly different pH–CBT relationship from the others: the wettest and
360 driest soils – Acrisols, Alisols, Ferralsols, Podzols, Regosols and Umbrisols –

361 could be distinguished from another group comprising Cambisols, Fluvisols
362 and Leptosols based on their pH–CBT slopes and associated standard errors
363 (Table 1). In addition, some soil types such as Alisols, Fluvisols, Phaeozems
364 and Regosols had peculiar MAAT–MBT'/CBT relationships when compared
365 with most other soil types (Table 1). This suggests that high soil
366 heterogeneity has an impact on (acido)bacterial communities involved in
367 brGDGT production (Jones et al., 2009) and that different communities may
368 respond in different ways to environmental changes.

369 The soil type effect on brGDGTs and their producers is also supported
370 by the different distributions of MAAT residuals per soil type (Fig. 4A), as
371 well as pH residuals per soil type to a lesser extent (data not shown). Six
372 soil types had mainly negative residuals, two soil types had mainly positive
373 residuals and four soil types had roughly equal numbers of positive as
374 negative residuals (Fig. 4A). These three groups of soil types in terms of
375 MAAT residuals were not distinguished by their typical moisture regimes
376 (Fig. 4A, Supplementary Table S1). In addition, some soil types such as
377 Alisols and Podzols had very high MAAT residuals (Figs. 4A, 5A and 5B).
378 Thus, (almost) systematic biases on MAAT–pH reconstructions may occur
379 for a given soil type when using global soil calibrations. This also implies
380 that not all soil types contribute equally to global scatters (Figs. 4A, 5A, 5B
381 and Supplementary Fig. S1).

382

383 4.1.2. *Traditional vs improved chromatographic method: is there an impact*
384 *on the soil type effect?*

385 Using the soil samples reconsidered by De Jonge et al. (2014), we
386 assess if 5- and 6-methyl brGDGT producers are influenced by the very high
387 soil heterogeneity, following the hypothesis that 5- and 6-methyl brGDGTs
388 are not produced by the same microorganisms (De Jonge et al., 2014).
389 Regression coefficients and performances differed at times between different
390 soil types for traditional and newest MAAT–pH/brGDGT relationships
391 (Table 2). In addition, not all soil types had similar traditional and new
392 MAAT–pH/brGDGT relationships to the global ones. After the homogeneity
393 of slopes tests/ANCOVA, at least one soil type had a significantly different
394 pH–CBT, MAAT–MBT'_{5ME} and pH–CBT' relationship from the others (Table
395 2). Acrisols, Ferralsols, Podzols and Regosols could be distinguished from
396 Cambisols, Fluvisols and Leptosols by their pH–CBT slopes (Table 2). Some
397 soil types such as Fluvisols and Regosols had peculiar MAAT–MBT'/CBT
398 relationships when compared with most other soil types (Table 2). The main
399 soil types generally had similar MAAT–MBT'_{5ME} slopes, but Fluvisols had a
400 significantly higher intercept than the other soil types (Table 2). Cambisols,
401 Leptosols and Regosols could be distinguished from Fluvisols and Podzols by
402 their pH–CBT' slopes (Table 2). Thus, the effect of soil type on MAAT–
403 pH/brGDGT relationships remains significant when 5- and 6-methyl
404 brGDGTs are quantified separately.

405 When considering MAAT–MBT'_{5ME} instead of MAAT–MBT'/CBT per
406 soil type, R^2 changes varied between –0.4 and 0.2, and RMSEs changes
407 varied between –1.2 and 1.1 °C (Table 2). When considering pH–CBT'
408 instead of pH–CBT per soil type, R^2 changes varied between –0.5 and 0.8,
409 and RMSEs changes varied between –0.7 and 0.0 pH units (Table 2).
410 Therefore, MAAT–pH/brGDGT relationships per soil type – and in
411 particular, MAAT–brGDGT relationships – are not systematically improved
412 when 5- and 6-methyl brGDGTs are quantified separately. In addition, the
413 improvements or deteriorations of MAAT–pH/brGDGT relationships clearly
414 depend on soil type (Table 2).

415 Decreases in MAAT(pH) residuals per soil type were not very clear
416 when 5- and 6-methyl brGDGTs were quantified separately, except in
417 Regosols (Figs. 4B and 4C). A more detailed inspection of MAAT residual
418 distributions in Leptosols and in Regosols (Fig. 5C and E) revealed that
419 these two soil types had high and opposite MAAT residuals using the
420 MAAT–MBT'/CBT calibration of Peterse et al. (2012). When using the
421 MAAT–MBT'_{5ME} calibration of De Jonge et al. (2014), MAAT residuals of
422 four Regosols decreased much more than the other Regosols and Luvisols
423 (Fig. 5D and F). These four Regosols highlighted by De Jonge et al. (2014)
424 not only had MAP values ≤ 550 mm, but they also had very high 6-methyl
425 brGDGT relative abundances ($> 60\%$ of total brGDGTs; Supplementary
426 Table S1). Despite the more substantial MAAT residual reduction in
427 Regosols, MAAT residual distributions per soil type were still not all

428 similar, as there remained some soil types with high and/or mainly positive
429 or negative residuals (Fig. 4C).

430 Averaged MAP values per soil type varied between 472 and 1870 mm,
431 which suggests that moisture regime clearly depends on soil type. Likewise,
432 averaged soil pH values per soil type varied between 4.4 and 7.3 pH units,
433 whereas averaged 6-methyl brGDGT relative abundances per soil type
434 varied between 1.4 and 51.7% of total brGDGTs (Supplementary Table S1).
435 Regosols had on average the lowest MAP values, and the highest pH values
436 and 6-methyl brGDGT relative abundances (Supplementary Table S1),
437 which is consistent with the greatest improvement of their pH–brGDGT
438 relationship and the greatest decreases in MAAT(pH) residuals (Fig. 4B and
439 C, Table 2). Conversely, soil types with averaged MAP values > 1000 mm
440 had the lowest averaged pH values and 6-methyl brGDGT relative
441 abundances (Supplementary Table S1), so no improvement of MAAT–
442 pH/brGDGT relationships nor clear decrease in MAAT(pH) residuals was
443 expected. However, pH–brGDGT relationships were improved in the wettest
444 soils (Fig. 4B and C, Table 2). In addition, soil types with averaged MAP
445 values between 500 and 1000 mm showed no intermediate behaviors
446 between the wettest and the driest soils (Fig. 4B and C, Table 2). This likely
447 explains why the separate quantification of 5- and 6-methyl brGDGTs
448 barely reduces the soil type effect on brGDGTs.

449

450 4.2. *Fan Si Pan soil transect*

451 4.2.1. *BrGDGT-derived proxies*

452 BIT values in Fan Si Pan soils (Table 3) are close to the reported
453 mean soil BIT value of 0.90 ± 0.14 (Schouten et al., 2013) and are consistent
454 with those observed in wet and acidic soils (e.g., Weijers et al., 2006b;
455 Loomis et al., 2011; Dirghangi et al., 2013). For MAAT, only one Fan Si Pan
456 soil fell outside the global MAAT–MBT'/CBT RMSE of Peterse et al. (2012)
457 of 5 °C (Table 3). For pH, half of the Fan Si Pan soils fell outside the global
458 pH–CBT RMSE of Peterse et al. (2012) of 0.8 pH units (Table 3). As RSME
459 means that globally 66% of the soils will fall within this error range, Fan Si
460 Pan soils adhere quite well to the variabilities of the global soil calibration
461 dataset of Peterse et al. (2012), especially for MAAT–MBT'/CBT.

462 The absence of correlation between measured pH and CBT ($r = -0.11$,
463 $p = 0.67$, Fig. 6) when all Fan Si Pan soils are considered together is likely
464 due to their very small pH domain (3.5–4.7 pH units, Table 3) and/or to the
465 differential relationships per soil type (Fig. 6, Table 3). Indeed, CBT and
466 measured pH were anti-correlated in Acrisols/Alisols, positively correlated
467 in Umbrisols, and had no clear relationship in Podzols.

468 MAAT–pH reconstructions along the Fan Si Pan transect may be
469 substantially biased by the co-elution of 5- and 6-methyl brGDGTs due to
470 our chromatographic method. Indeed, Yang et al. (2015a) have shown that
471 6-methyl brGDGTs significantly deteriorate the performance of MBT' as a
472 MAAT/altitude proxy along Mt. Shennongjia, China. Additionally, MBT' is
473 not (well) correlated with MAAT/altitude along most other altitudinal

474 transects studied so far in China, India and Tanzania (Peterse et al., 2009b;
475 Yang et al., 2010; Ernst et al., 2013; Coffinet et al., 2014; Deng et al., 2016),
476 which may be due to 6-methyl brGDGTs as well. Conversely, soil depth
477 effect is not a plausible explanation as the soil samples considered for
478 altitudinal lapse rate studies were taken from surficial horizons.

479

480 *4.2.2. Soil type effect on brGDGTs: a focus on contrasting soil organic matter* 481 *properties*

482 For the Fan Si Pan surficial soils – sampled from horizons with a
483 mean soil depth < 10 cm – MBT' and MBT'/CBT-based MAAT mainly
484 decreased between the lowest and highest altitude soils, in particular
485 between the Podzols FAN4.1/FAN5.1 and the Umbrisols FAN6.1/FAN6.2
486 (Fig. 6, Table 3). Conversely, MAAT estimates did not decrease with altitude
487 between the Acrisol FAN1.1, the Alisols FAN2.A0/FAN2.1 and the Podzol
488 FAN4.1. Despite our difficulties in separating the effects of vegetation/soil
489 type and adiabatic cooling on brGDGT distributions along the Fan Si Pan
490 transect, the absence of a decrease in MAAT estimates between the four
491 lowest altitude soils suggests the importance of the diversity of soils
492 encountered along this transect.

493 The different main soil types present along the Fan Si Pan transect
494 have contrasting C_{org} sources, stocks and mineralization rates (Podwojewski
495 et al., 2011). In the Fan Si Pan Acrisols, C_{org} has a rapid turnover due to
496 relatively high temperatures and constant inputs from leaves, resulting in a

497 thin litter layer and rapid C_{org} mineralization. In the Fan Si Pan Podzols,
498 C_{org} decomposition rate is lower, partially due to cooler temperatures and
499 seasonal inputs from leaves (Podwojewski et al., 2011). The Fan Si Pan
500 Podzols thus have a thicker litter layer, resulting in very high topsoil C_{org}
501 stocks. In addition, the second major change in vegetation type along the
502 Fan Si Pan transect has induced the transition from Podzols to Umbrisols
503 with a thinning of the litter layer, resulting in lower topsoil C_{org} stocks and a
504 different C_{org} source (Fig. 2B; Podwojewski et al., 2011). Indeed, C_{org} inputs
505 for Podzols are exogenic – mainly from the thick litter layer – whereas C_{org}
506 inputs for Umbrisols are endogenic, mainly from bamboo roots and thus
507 more homogenous.

508 Substantial changes in C_{org} sources, stocks and/or mineralization
509 rates in soils may induce changes in substrate nature and/or nutrient
510 availability for brGDGT producers, which may modify brGDGT distributions
511 and so bias MAAT–pH reconstructions, as suggested by previous workers
512 such as Anderson et al. (2014). Thus, biases due to vegetation and soil types
513 should be jointly investigated, preferentially along lateral and local soil
514 transects with as many constant environmental parameters as possible,
515 such as MAAT, soil temperature, vegetation type and parent material.

516

517 *4.2.3. Effects of soil depth on brGDGT-derived proxies*

518 The soil collection of the Fan Si Pan transect allows to investigate five
519 well-studied soil profiles. Substantially lower brGDGT-based MAATs in

520 deep soils as opposed to topsoils were reported in two Podzol profiles under
521 different climates (Huguet et al., 2010), a trend that also occurred in the
522 Fan Si Pan Podzol profiles, but not in the other Fan Si Pan soil profiles (Fig.
523 6). Likewise, changes in CBT-based pH with depth were not similar between
524 the different Fan Si Pan soil profiles (Fig. 6). We do not know to what extent
525 (acido)bacterial communities change with depth in the different Fan Si Pan
526 soil profiles nor to what extent such changes impact brGDGT distributions
527 in soils. For this reason, we put forward various explanations for the
528 observed changes in brGDGT distributions with soil depth.

529 Every Fan Si Pan sample was 2-mm sieved (Podwojewski et al.,
530 2011), meaning that root-associated brGDGTs in subsoils (Huguet et al.,
531 2013b) cannot explain the decreased MAAT estimates in the deep Fan Si
532 Pan Podzols. Nevertheless, given that bamboo roots (abundant in the
533 Umbrisol profile FAN 6) are more mineralizable than tree roots (abundant
534 in the Podzol profiles FAN 4 and FAN 5), brGDGT producing communities
535 may change differently with depth between the main Fan Si Pan soil types,
536 resulting in differential associated biases on MAAT–pH estimates, following
537 the hypothesis that different (acido)bacterial species do not all produce the
538 same brGDGTs (Sinninghe Damsté et al., 2011, 2014; De Jonge et al., 2014).
539 Alternatively, Podzols have the peculiarity of having a subsoil enriched in
540 Fe, Al and organic matter – including lipids – due to rainwater percolation
541 (e.g., Huguet et al., 2010; Podwojewski et al., 2011). Therefore, substantial
542 changes with depth in biotic and abiotic processes not related to brGDGT

543 producers – for instance, lipid transfer to a non-extractable pool via organo-
544 metallic complexation – may occur in podzol soils (e.g., Huguet et al., 2010).
545 Nevertheless, such processes – which also include soil bioturbation by soil
546 fauna and soil reworking by rooted trees – are unlikely to be restricted to
547 Podzols.

548 BrGDGT distributions may also be influenced by the history of the
549 soils. Former agricultural activities – mainly maize crops (Fig. 2B;
550 Podwojewski et al., 2011) – may have impacted brGDGT distributions in the
551 FAN 1 soil profile. Additionally, the transition from primary broad-leaved
552 forests to alpine vegetation (Fig. 2B; Podwojewski et al., 2011) has shifted
553 upwards in altitude under the effect of the present global warming (IPCC,
554 2013). This transition is now close to the FAN 6 site, which may thus have
555 experienced a major temporal change in vegetation type. However, the
556 brGDGT turnover times reported so far – from a few months to less than 45
557 years (Peterse et al., 2010; Weijers et al., 2010; Huguet et al., 2013a) – may
558 be true for surficial soils only. Indeed, brGDGTs may be associated with the
559 mineral phase and/or be incorporated within the macromolecular matrix in
560 deeper soil horizons (e.g., Huguet et al., 2010), whereas microbial activity
561 may decrease with depth, resulting in substantially longer brGDGT
562 turnover times in deep soils. The latter is suggested by decreases in C_{org} -
563 normalized brGDGT absolute abundances with depth in FAN 1, FAN 2 and
564 FAN 4 (data not shown). Additionally, imprints of former communities may
565 be muted by the post-depositional effect (e.g., Zech et al., 2012; Yamamoto et

566 al., 2016), and such an effect is indeed suggested by an increase in C_{org} -
567 normalized brGDGT absolute abundances with depth in FAN 6 (data not
568 shown).

569

570 **5. Conclusions and perspectives**

571 Soil types were assigned to a composite global dataset of 358 soils to
572 investigate MAAT–pH/brGDGT relationships and MAAT(pH) residuals per
573 soil type. Distributions of brGDGTs were also investigated in five soil
574 profiles excavated along an altitudinal transect in the Mount Fan Si Pan
575 National Park. Surrounding vegetation, geological setting, as well as soil
576 sequence had previously been intensively characterized, providing an
577 opportunity to investigate their impact on proxies intensively used in paleo-
578 studies.

579 The soil type diversity of the global dataset was high, traditional
580 MAAT–pH/relationships per soil type were not all similar and different soil
581 types (e.g., Alisols and Podzols) did not all provide the same contribution to
582 global MAAT(pH)/brGDGT scatters. Additionally, the soil type effect on
583 MAAT–pH relationships remained significant when 5- and 6-methyl
584 brGDGTs were quantified separately and no obvious reduction in
585 MAAT(pH) residuals per soil type occurred in general (e.g., in Leptosols,
586 which contained 6-methyl brGDGTs). In the Mount Fan Si Pan National
587 Park, MBT/CBT-based MAATs were not significantly different to modeled
588 MAATs when the global calibration error of 5 °C was taken into account.

589 However, the decrease in MAAT estimates along the altitudinal transect
590 lacked clarity when the focus was on surficial soils, and the pH–CBT
591 relationship was absent when all Fan Si Pan soils were considered. On the
592 one hand, substantial changes in soil/vegetation type along the Fan Si Pan
593 transect may induce biases on MAAT–pH reconstructions in surficial soils.
594 On the other hand, MBT'/CBT indices varied slightly or substantially with
595 depth in the Fan Si Pan soil profiles, possibly as a function of soil type and
596 history.

597 To better understand the biases on brGDGT-based estimates, more
598 soil profiles should be investigated along topo-sequences, as attempted in
599 our work. Indeed, this study reveals the importance of direct collaborations
600 between organic geochemists and pedologists, ensuring that specific organic
601 compounds and physico-chemical soil properties are jointly investigated. To
602 consider the evolution of soil properties through time, as well as the transfer
603 time of soil C_{org}, radiocarbon analyses on bulk soil C_{org} and on specific
604 organic compounds should be conducted. Additionally, future
605 global/regional/local soil MAAT–pH/brGDGT calibrations should consider
606 sample sizes of a few dozen to a few hundred per soil type to ensure
607 adequate specificity for all given soil types.

608

609 **Acknowledgements**

610 G.M. thanks Anneke de Rouw and the HYDRARIDE consortium for
611 making this study and the connection with pedologists possible through

612 discussions in the field in Cameroon. Work at CEREGE is supported by
613 ECCOREV FR3098 (project ECCOTEMP) and the Collège de France. N.D.
614 thanks Ecole Normale Supérieure de Lyon for providing salary support. We
615 are grateful to two anonymous reviewers for their constructive suggestions
616 that greatly helped us to considerably improve this manuscript.

617

618 **Appendix A. Supplementary material.**

619

620 *Associate Editor*—**Klaas Nierop**

621

622 **References**

- 623 Anderson, V.J., Shanahan, T.M., Saylor, J.E., Horton, B.K., Mora, A.R.,
624 2014. Sources of local and regional variability in the MBT'/CBT
625 paleotemperature proxy: Insights from a modern elevation transect
626 across the Eastern Cordillera of Colombia. *Organic Geochemistry* 69,
627 42–51.
- 628 Coffinet, S., Hugué, A., Williamson, D., Fosse, C., Derenne, S., 2014.
629 Potential of GDGTs as a temperature proxy along an altitudinal
630 transect at Mount Rungwe (Tanzania). *Organic Geochemistry* 68, 82–
631 89.
- 632 Dang, X., Yang, H., Naafs, B.D.A., Pancost, R.D., Xie, S., 2016. Evidence of
633 moisture control on the methylation of branched glycerol dialkyl

634 glycerol tetraethers in semi-arid and arid soils. *Geochimica et*
635 *Cosmochimica Acta* 189, 24–36.

636 De Jonge, C., Hopmans, E.C., Zell, C.I., Kim, J.-H., Schouten, S., Sinninghe
637 Damsté, J.S., 2014. Occurrence and abundance of 6-methyl branched
638 glycerol dialkyl glycerol tetraethers in soils: Implications for
639 palaeoclimate reconstruction. *Geochimica et Cosmochimica Acta* 141,
640 97–112.

641 Deng, L., Jia, G., Jin, C., Li, S., 2016. Warm season bias of branched GDGT
642 temperature estimates causes underestimation of altitudinal lapse
643 rate. *Organic Geochemistry* 96, 11–17.

644 Dirghangi, S.S., Pagani, M., Hren, M.T., Tipple, B.J., 2013. Distribution of
645 glycerol dialkyl glycerol tetraethers in soils from two environmental
646 transects in the USA. *Organic Geochemistry* 59, 49–60.

647 Ernst, N., Peterse, F., Breitenbach, S.F.M., Syiemlieh, H.J., Eglinton, T.I.,
648 2013. Biomarkers record environmental changes along an altitudinal
649 transect in the wettest place on Earth. *Organic Geochemistry* 60, 93–
650 99.

651 Fox, J., Weisberg, S., 2011. *An {R} Companion to Applied Regression*,
652 Second edition. Sage, Thousand Oaks CA, USA.
653 <http://socserv.socsci.mcmaster.ca/jfox/Books/Companion>.

654 Hengl, T., de Jesus, J.M., MacMillan, R.A., Batjes, N.H., Heuvelink, G.B.M.,
655 Ribeiro, E., Samuel-Rosa, A., Kempen, B., Leenaars, J.G.B., Walsh,

656 M.G., Gonzalez, M.R., 2014. SoilGrids1km — Global soil information
657 based on automated mapping. PLoS ONE 9, e105992.

658 Hopmans, E.C., Weijers, J.W.H., Schefuß, E., Herfort, L., Sinninghe
659 Damsté, J.S., Schouten, S., 2004. A novel proxy for terrestrial organic
660 matter in sediments based on branched and isoprenoid tetraether
661 lipids. Earth and Planetary Science Letters 224, 107–116.

662 Huguet, A., Fosse, C., Metzger, P., Fritsch, E., Derenne, S., 2010.
663 Occurrence and distribution of extractable glycerol dialkyl glycerol
664 tetraethers in podzols. Organic Geochemistry 41, 291–301.

665 Huguet, A., Fosse, C., Laggoun-Défarge, F., Delarue, F., Derenne, S., 2013a.
666 Effects of a short-term experimental microclimate warming on the
667 abundance and distribution of branched GDGTs in a French
668 peatland. Geochimica et Cosmochimica Acta 105, 294–315.

669

670 Huguet, A., Gocke, M., Derenne, S., Fosse, C., Wiesenberg, G.L.B., 2013b.
671 Root-associated branched tetraether source microorganisms may
672 reduce estimated paleotemperatures in subsoil. Chemical Geology
673 356, 1–10.

674 IPCC, 2013. Climate change 2013: The physical science basis. Contribution
675 of Working Group I to the Fifth Assessment Report of the
676 Intergovernmental Panel on Climate Change [Stocker, T.F., Qin, D.,
677 Plattner, G.-K., Tignor, M., Allen, S.K., Boschung, J., Nauels, A., Xia,

678 Y., Bex, V., Midgley, P.M. (eds.)]. Cambridge University Press,
679 Cambridge, United Kingdom and New York, NY, USA.

680 IUSS Working Group WRB, 2015. World Reference Base for Soil Resources
681 2014, update 2015. International soil classification system for naming
682 soils and creating legends for soil maps. World Soil Resources Reports
683 No. 106. FAO, Rome.

684 Jones, R.T., Robeson, M.S., Lauber, C.L., Hamady, M., Knight, R., Fierer,
685 N., 2009. A comprehensive survey of soil acidobacterial diversity
686 using pyrosequencing and clone library analyses. *The ISME Journal*
687 3, 442–453.

688 Liu, W., Wang, H., Zhang, C.L., Liu, Z., He, Y., 2013. Distribution of glycerol
689 dialkyl glycerol tetraether lipids along an altitudinal transect on Mt.
690 Xiangpi, NE Qinghai-Tibetan Plateau, China. *Organic Geochemistry*
691 57, 76–83.

692 Loomis, S.E., Russell, J.M., Sinninghe Damsté, J.S., 2011. Distributions of
693 branched GDGTs in soils and lake sediments from western Uganda:
694 Implications for a lacustrine paleothermometer. *Organic*
695 *Geochemistry* 42, 739–751.

696 Menges, J., Huguet, C., Alcañiz, J.M., Fietz, S., Sachse, D., Rosell-Melé, A.,
697 2014. Influence of water availability in the distributions of branched
698 glycerol dialkyl glycerol tetraether in soils of the Iberian Peninsula.
699 *Biogeosciences* 11, 2571–2581.

700 Nieto-Moreno, V., Rohrmann, A., van der Meer, M.T.J., Sinninghe Damsté,
701 J.S., Sachse, D., Tofelde, S., Niedermeyer, E.M., Strecker, M.R.,
702 Mulch, A., 2016. Elevation-dependent changes in *n*-alkane δ D and soil
703 GDGTs across the South Central Andes. *Earth and Planetary Science*
704 *Letters* (in press). <http://dx.doi.org/10.1016/j.epsl.2016.07.049>.

705 Peterse, F., Nicol, G.W., Schouten, S., Sinninghe Damsté, J.S., 2010.
706 Influence of soil pH on the abundance and distribution of core and
707 intact polar lipid-derived branched GDGTs in soil. *Organic*
708 *Geochemistry* 41, 1171–1175.

709 Peterse, F., Schouten, S., van der Meer, M.T.J., Sinninghe Damsté, J.S.,
710 2009a. Distribution of branched tetraether lipids in geothermally
711 heated soils: Implications for the MBT/CBT temperature proxy.
712 *Organic Geochemistry* 40, 201–205.

713 Peterse, F., van der Meer, M.T.J., Schouten, S., Jia, G., Ossebaar, J.,
714 Blokker, J., Sinninghe Damsté, J.S., 2009b. Assessment of soil *n*-
715 alkane δ D and branched tetraether membrane lipid distributions as
716 tools for paleoelevation reconstruction. *Biogeosciences* 6, 2799–2807.

717 Peterse, F., van der Meer, J., Schouten, S., Weijers, J.W.H., Fierer, N.,
718 Jackson, R.B., Kim, J.-H., Sinninghe Damsté, J.S., 2012. Revised
719 calibration of the MBT–CBT paleotemperature proxy based on
720 branched tetraether membrane lipids in surface soils. *Geochimica et*
721 *Cosmochimica Acta* 96, 215–229.

722 Podwojewski, P., Poulénard, J., Nguyet, M.L., de Rouw, A., Nguyen, V.T.,
723 Pham, Q.H., Tran, D.T., 2011. Climate and vegetation determine soil
724 organic matter status in an alpine inner-tropical soil catena in the
725 Fan Si Pan Mountain, Vietnam. *Catena* 87, 226–239.

726 R Development Core Team, 2016. R: A language and environment for
727 statistical computing. R Foundation for Statistical Computing,
728 Vienna, Austria. ISBN 3-900051-07-0, url: <http://www.R-project.org>.

729 Sanchi, L., Ménot, G., Bard, E., 2014. Insights into continental
730 temperatures in the northwestern Black Sea area during the Last
731 Glacial period using branched tetraether lipids. *Quaternary Science*
732 *Reviews* 84, 98–108.

733 Sanchi, L., Ménot, G., Bard, E., 2013. An automated purification method for
734 archaeal and bacterial tetraethers in soils and sediments. *Organic*
735 *Geochemistry* 54, 83–90.

736 Schouten, S., Hopmans, E.C., Sinninghe Damsté, J.S., 2013. The organic
737 geochemistry of glycerol dialkyl glycerol tetraether lipids: A review.
738 *Organic Geochemistry* 54, 19–61.

739 Sinninghe Damsté, J.S., Ossebaar, J., Schouten, S., Verschuren, D., 2008.
740 Altitudinal shifts in the branched tetraether lipid distribution in soil
741 from Mt. Kilimanjaro (Tanzania): Implications for the MBT/CBT
742 continental palaeothermometer. *Organic Geochemistry* 39, 1072–
743 1076.

744 Sinninghe Damsté, J.S., Rijpstra, W.I.C., Hopmans, E.C., Foesel, B.U.,
745 Wüst, P.K., Overmann, J., Tank, M., Bryant, D.A., Dunfield, P.F.,
746 Houghton, K., Stott, M.B., 2014. Ether- and ester-bound *iso*-diabolic
747 acid and other lipids in members of *Acidobacteria* subdivision 4.
748 Applied and Environmental Microbiology 80, 5207–5218.

749 Sinninghe Damsté, J.S., Rijpstra, W.I.C., Hopmans, E.C., Weijers, J.W.H.,
750 Foesel, B.U., Overmann, J., Dedysh, S.N., 2011. 13,16-Dimethyl
751 octacosanedioic acid (*iso*-diabolic acid), a common membrane-
752 spanning lipid of *Acidobacteria* subdivisions 1 and 3. Applied and
753 Environmental Microbiology 77, 4147–4154.

754 Smerdon, J.E., Pollack, H.N., Cermak, V., Enz, J.W., Kresl, M., Safanda, J.,
755 Wehmiller, J.F., 2004. Air-ground temperature coupling and
756 subsurface propagation of annual temperature signals. Journal of
757 Geophysical Research 109, D21107.

758 Wang, H., Liu, W., Lu, H., 2016. Appraisal of branched glycerol dialkyl
759 glycerol tetraether-based indices for North China. Organic
760 Geochemistry 98, 118–130.

761

762 Weijers, J.W.H., Schouten, S., Hopmans, E.C., Geenevasen, J.A.J., David,
763 O.R.P., Coleman, J.M., Pancost, R.D., Sinninghe Damsté, J.S., 2006a.
764 Membrane lipids of mesophilic anaerobic bacteria thriving in peats
765 have typical archaeal traits. Environmental Microbiology 8, 648–657.

766 Weijers, J.W.H., Schouten, S., Spaargaren, O.C., Sinninghe Damsté, J.S.,
767 2006b. Occurrence and distribution of tetraether membrane lipids in
768 soils: Implications for the use of the TEX₈₆ proxy and the BIT index.
769 *Organic Geochemistry* 37, 1680–1693.

770 Weijers, J.W.H., Schouten, S., van den Donker, J.C., Hopmans, E.C.,
771 Sinninghe Damsté, J.S., 2007. Environmental controls on bacterial
772 tetraether membrane lipid distribution in soils. *Geochimica et*
773 *Cosmochimica Acta* 71, 703–713.

774 Weijers, J.W.H., Panoto, E., van Bleijswijk, J., Schouten, S., Rijpstra,
775 W.I.C., Balk, M., Stams, A.J.M., Sinninghe Damsté, J.S., 2009.
776 Constraints on the biological source(s) of the orphan branched
777 tetraether membrane lipids. *Geomicrobiology Journal* 26, 402–414.

778 Weijers, J.W.H., Wiesenberg, G.L.B., Bol, R., Hopmans, E.C., Pancost, R.D.,
779 2010. Carbon isotopic composition of branched tetraether membrane
780 lipids in soils suggest a rapid turnover and a heterotrophic life style
781 of their source organism(s). *Biogeosciences* 7, 2959–2973.

782 Yamamoto, Y., Ajioka, T., Yamamoto, M., 2016. Climate reconstruction
783 based on GDGT-based proxies in a paleosol sequence in Japan:
784 Postdepositional effect on the estimation of air temperature.
785 *Quaternary International* 397, 380–391.

786 Yang, H., Ding, W., He, G., Xie, S., 2010. Archaeal and bacterial tetraether
787 membrane lipids in soils of varied altitudes in Mt. Jianfengling in
788 South China. *Journal of Earth Science* 21, 277–280.

789 Yang, H., Lü, X., Ding, W., Lei, Y., Dang, X., Xie, S., 2015a. The 6-methyl
790 branched tetraethers significantly affect the performance of the
791 methylation index (MBT') in soils from an altitudinal transect at
792 Mount Shennongjia. *Organic Geochemistry* 82, 42–53.

793 Yang, H., Xiao, W., Jia, C., Xie, S., 2015b. Paleoaltimetry proxies based on
794 bacterial branched tetraether membrane lipids in soils. *Frontiers of*
795 *Earth Science* 9, 13–25.

796 Zech, R., Gao, L., Tarozo, R., Huang, Y., 2012. Branched glycerol dialkyl
797 glycerol tetraethers in Pleistocene loess-paleosol sequences: Three
798 case studies. *Organic Geochemistry* 53, 38–44.

799 Zhuang, G., Pagani, M., Chamberlin, C., Strong, D., Vandergoes, M., 2015.
800 Altitudinal shift in stable hydrogen isotopes and microbial tetraether
801 distribution in soils from the Southern Alps, NZ: Implications for
802 paleoclimatology and paleoaltimetry. *Organic Geochemistry* 79, 56–
803 64.

804

805 **Figure captions**

806 **Fig. 1.** Structures of crenarchaeol (Cren), 5-methyl (Roman numbers with
807 no prime symbol) and 6-methyl (Roman numbers with a prime symbol)
808 branched glycerol dialkyl glycerol tetraethers (brGDGTs, I-II-III) with the
809 different $\alpha 5$ and/or $\omega 5$ positions and the different $\alpha 6$ and/or $\omega 6$ positions of
810 the methyl groups.

811

812 **Fig. 2.** (A) Maps showing the locations of the study site (left-hand map) and
813 the studied soil profiles (right-hand map). Contour interval is 200 m and
814 contour lines indicate altitudes between 1000 and 3000 m on the right-hand
815 map, with darker tones for higher altitudes. Modified from maps generated
816 from GeoMapApp (<http://www.geomapapp.org>). (B) Profile showing the
817 studied soil pits. Altitudinal zonation of vegetation types is indicated in
818 green. The profile does not pass exactly through the soil pits, which explains
819 why their altitudes in the profile do not correspond to their actual altitudes.
820 Horizons are delimited and color-coded as per the samples taken by
821 Podwojewski et al. (2011): orange-yellow tones for A horizons, blue tones for
822 Bw horizons and green tones for Bs horizons. Like tones correspond to like
823 horizons. The horizons considered for soil brGDGT distributions are
824 indicated in red. Adapted from Podwojewski et al. (2011).

825

826 **Fig. 3.** BrGDGT-derived proxy data from the composite global soil dataset
827 (Huguet et al., 2010; Peterse et al., 2012; Dirghangi et al., 2013; Anderson et

828 al., 2014; De Jonge et al., 2014), with 27 soil types being distinguished. (A)
829 Instrumental/modeled mean annual air temperature (MAAT) vs MBT'/CBT.
830 (B) Instrumental/modeled MAAT vs MBT'_{5ME}. (C) Measured pH vs CBT. (D)
831 Measured pH vs CBT'. The outliers are also shown in each plot. The red
832 lines in plots (B), (C) and (D) correspond to the global linear regressions on
833 the composite global soil dataset after outlier removal.

834

835 **Fig. 4.** Box-whisker plots of mean annual air temperature (MAAT) residuals
836 per soil type showing minima and maxima with whiskers, medians with
837 horizontal bars, 1st and 3rd quartiles with boxes, and means with pluses.
838 Plot (A) is based on the composite global soil dataset (Huguet et al., 2010;
839 Peterse et al., 2012; Dirghangi et al., 2013; Anderson et al., 2014; De Jonge
840 et al., 2014). Plots (B) and (C) are based on the soils reconsidered by De
841 Jonge et al. (2014). In plots (A) and (B), residuals are based on the MAAT–
842 MBT'/CBT global soil calibration of Peterse et al. (2012). In plot (C),
843 residuals are based on the MAAT–MBT'_{5ME} global soil calibration of De
844 Jonge et al. (2014). Only soil types comprising at least 10 soils from the
845 global datasets are considered. When outliers are identified for a given soil
846 type, their number is indicated as (initial number of samples – number of
847 outliers) below the number of samples actually considered. Moisture
848 regimes based on averaged mean annual precipitation (MAP) values per soil
849 type are specified with the following color-coding of the numbers of samples

850 per soil type: blue if MAP > 1000 mm, orange if MAP 500–1000 mm and red
851 if MAP < 500 mm.

852

853 **Fig. 5.** Mean annual air temperature (MAAT) residual distributions for (A)
854 Podzols, (B) Alisols, (C) and (D) Leptosols, and (E) and (F) Regosols. Plots
855 (A) and (B) are based on the composite global soil dataset (Huguet et al.,
856 2010; Peterse et al., 2012; Dirghangi et al., 2013; Anderson et al., 2014; De
857 Jonge et al., 2014). Plots (C), (D), (E) and (F) are based on the soils
858 reconsidered by De Jonge et al. (2014). In plots (A), (B), (C) and (E),
859 residuals are based on the MAAT–MBT'/CBT global soil calibration of
860 Peterse et al. (2012). In plots (D) and (F), residuals are based on the MAAT–
861 MBT'_{5ME} global soil calibration of De Jonge et al. (2014). Gaussians indicate
862 the mean values with their standard deviations. Filled circles represent the
863 medians and filled diamonds represent the extreme values and the 1st and
864 3rd quartiles. When outliers are identified for a given soil type, their number
865 is indicated as (initial number of samples – number of outliers) below the
866 number of samples actually considered.

867

868 **Fig. 6.** BIT (Hopmans et al., 2004), MBT' (Peterse et al., 2012), CBT
869 (Weijers et al., 2007), and MBT'/CBT-derived mean annual air temperature
870 (MAAT) and pH based on the extended soil calibration (Peterse et al., 2012)
871 in the studied Fan Si Pan soil profiles. Modeled MAAT and measured pH
872 (Podwojewski et al., 2011 for the latter) are shown for comparison. Horizons

873 are delimited and color-coded as described in the caption for Fig. 2B.
874 Symbols with error bars next to axis titles represent mean 1- σ standard
875 deviations to mean values of duplicates. Surficial horizons, with a mean
876 depth < 10 cm, are indicated in red.

877

878 **Table captions**

879 **Table 1**

880 Number of samples (n), coefficients (a, b, c, S, I and R^2), and root mean
881 square errors (E) of traditional mean annual air temperature (MAAT)–
882 pH/brGDGT linear regressions per soil type using the composite global soil
883 dataset (Huguet et al., 2010; Peterse et al., 2012; Dirghangi et al., 2013;
884 Anderson et al., 2014; De Jonge et al., 2014). Only soil types comprising at
885 least 10 soils from the global dataset are considered for the linear
886 regressions. When outliers are identified for a given MAAT–pH/brGDGT
887 relationship per soil type, their number is indicated as (initial number of
888 samples – number of outliers) next to the number of samples actually
889 considered. Statistical significance is reached for p -values < 0.05.

890

891 **Table 2**

892 Number of samples (n), coefficients (a, b, c, S, I and R^2), and root mean
893 square errors (E) of traditional and newest mean annual air temperature
894 (MAAT)–pH/brGDGT linear regressions per soil type using the soils of the
895 composite global soil dataset (Huguet et al., 2010; Peterse et al., 2012;

896 Dirghangi et al., 2013; Anderson et al., 2014; De Jonge et al., 2014)
897 reconsidered by De Jonge et al. (2014). Only soil types comprising at least 10
898 soils from the global dataset are considered for the linear regressions. When
899 outliers are identified for a given MAAT–pH/brGDGT relationship per soil
900 type, their number is indicated as (initial number of samples – number of
901 outliers) next to the number of samples actually considered. Statistical
902 significance is reached for p -values < 0.05 .

903

904 **Table 3**

905 BrGDGT-derived proxies and MBT'/CBT-derived mean annual air
906 temperature (MAAT) and pH based on the extended soil calibration (Peterse
907 et al., 2012) along the Fan Si Pan Mountain transect. Altitude, coordinates,
908 horizon, mean depth, organic carbon (C_{org}) concentration, water content
909 (H_2O), and measured pH are from Podwojewski et al. (2011). nd = not
910 determined.

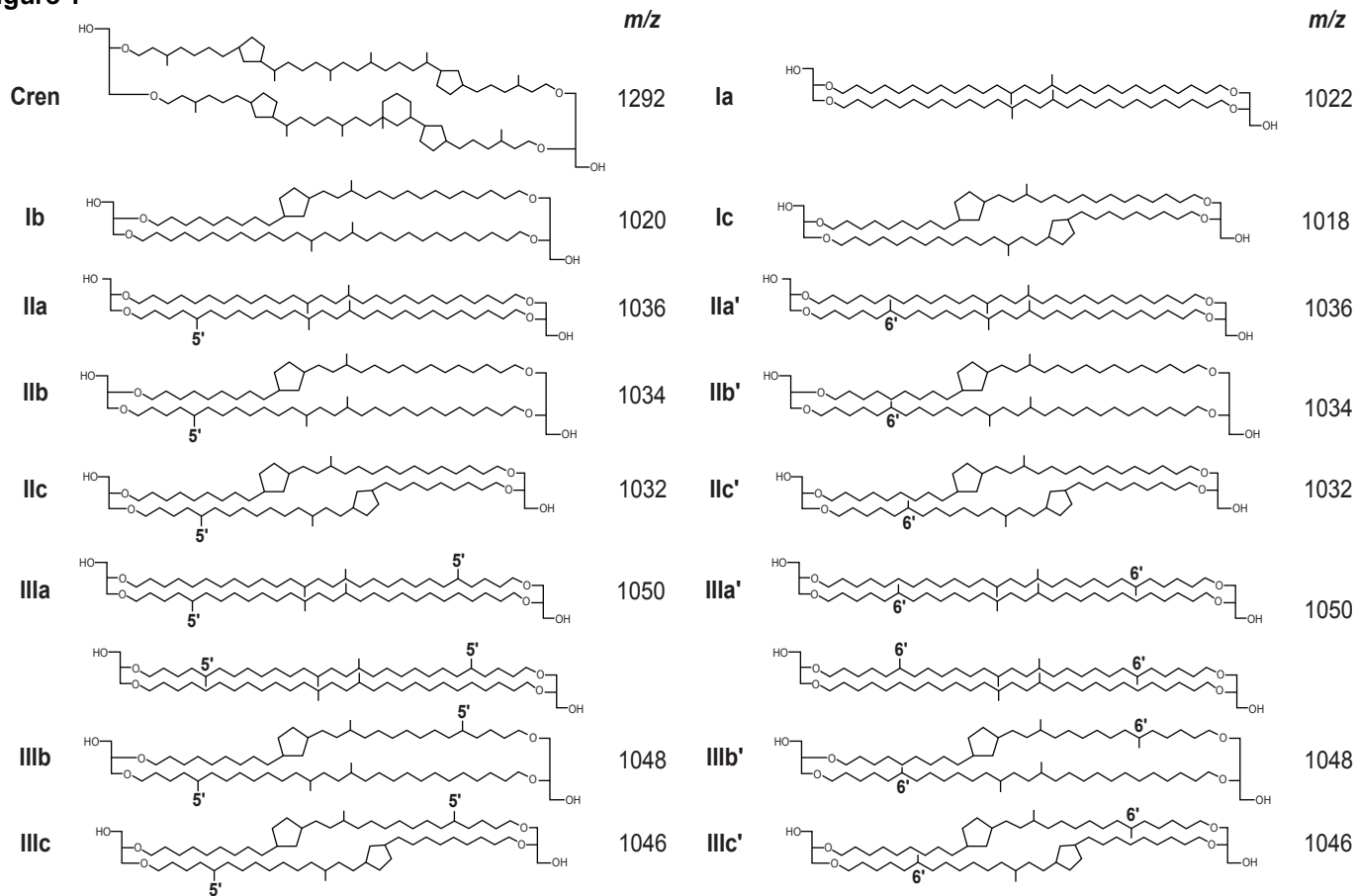
Figure 1

Figure 2 - revised

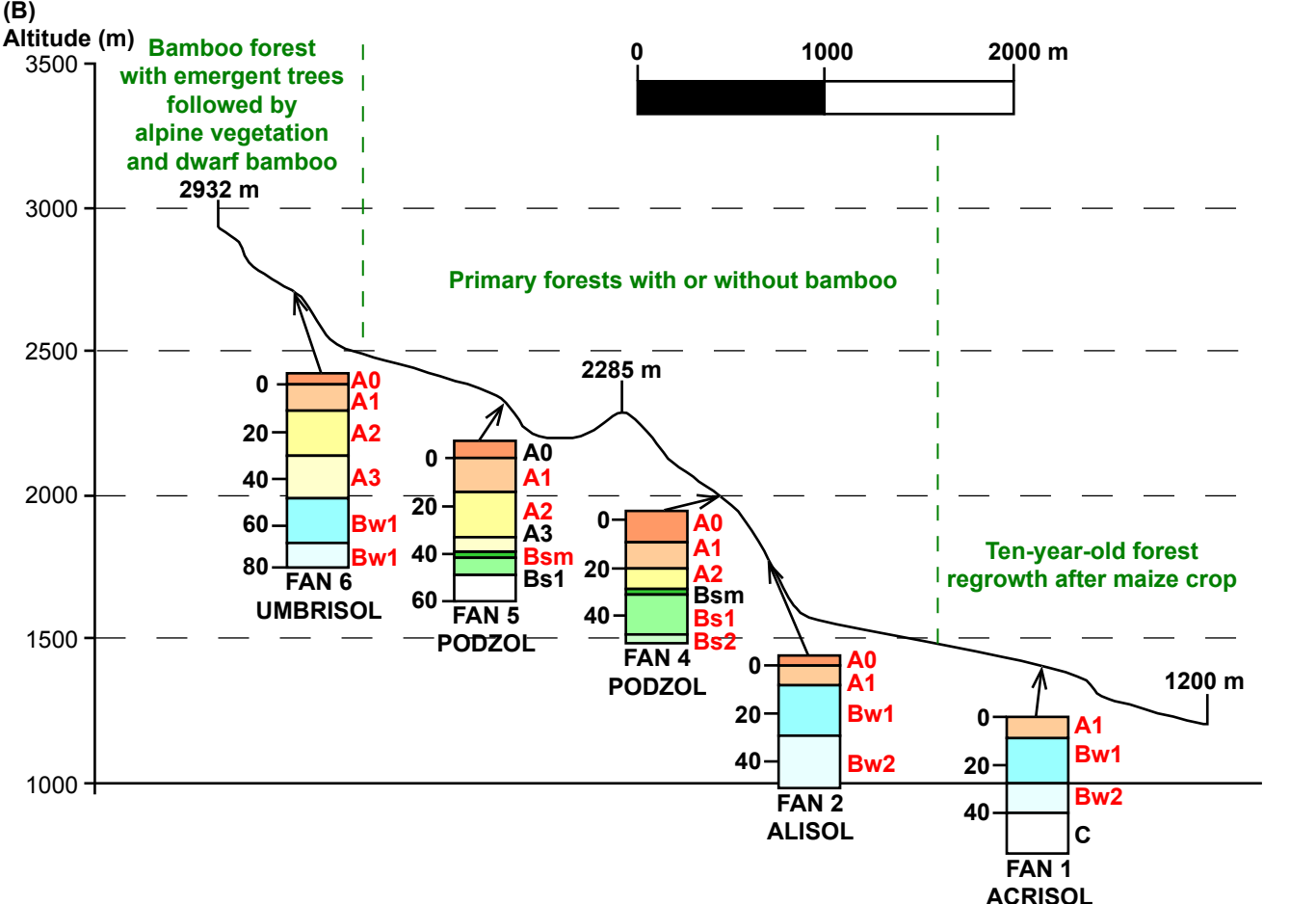
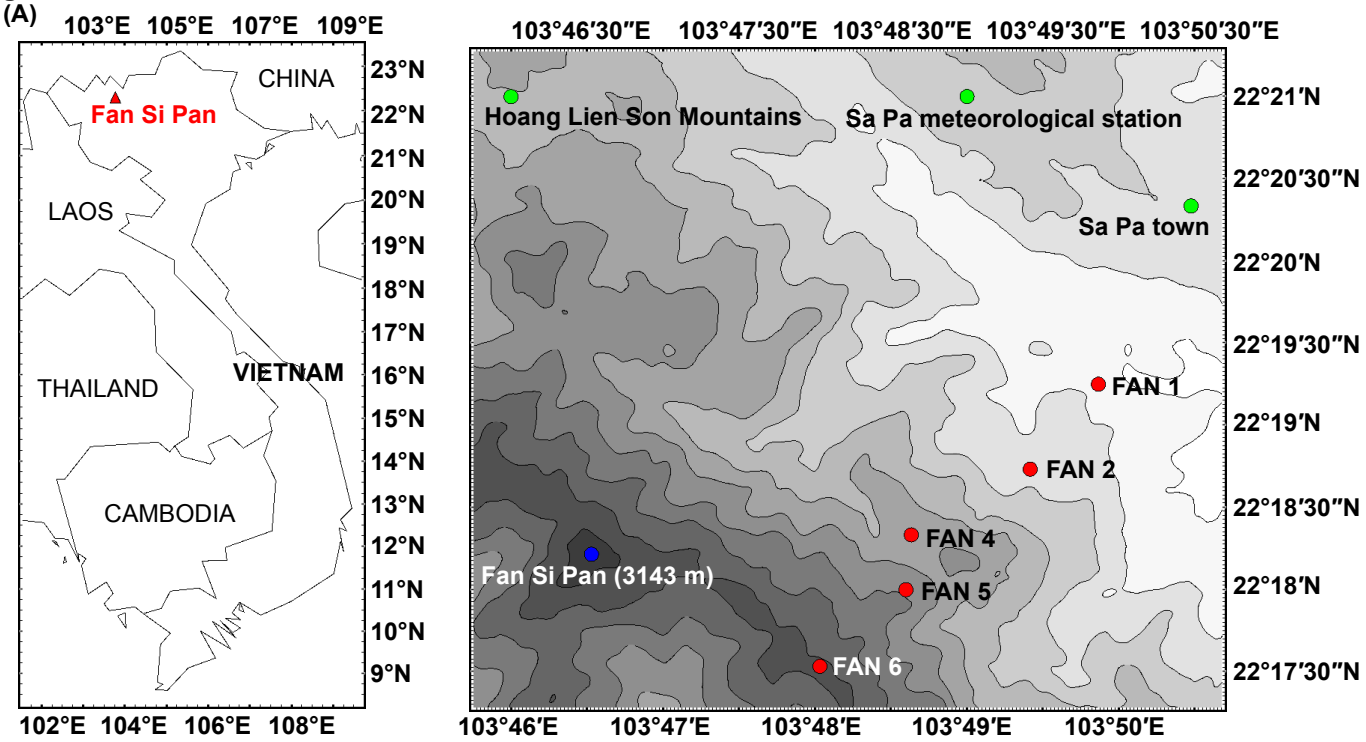


Figure 3 - revised

- | | | | | | | | | | | | | | |
|---|-----------|---|-----------|---|----------|---|-------------|---|------------|---|----------|---|------------|
| + | Luvisol | ▲ | Lixisol | ◆ | Nitisol | ◇ | Cambisol | ○ | Cryosol | ★ | Histosol | ◇ | Umbrisol |
| ◆ | Acrisol | ✱ | Anthrosol | ✕ | Podzol | + | Phaeozem | △ | Andosol | ▣ | Planosol | ■ | Kastanozem |
| ■ | Vertisol | ▼ | Ferralsol | ✱ | Fluvisol | ◇ | Albeluvisol | ⊠ | Arenosol | ▽ | Calcisol | ✱ | Chernozem |
| ● | Solonchak | ▲ | Gleysol | ★ | Alisol | □ | Leptosol | × | Plinthosol | □ | Regosol | | |

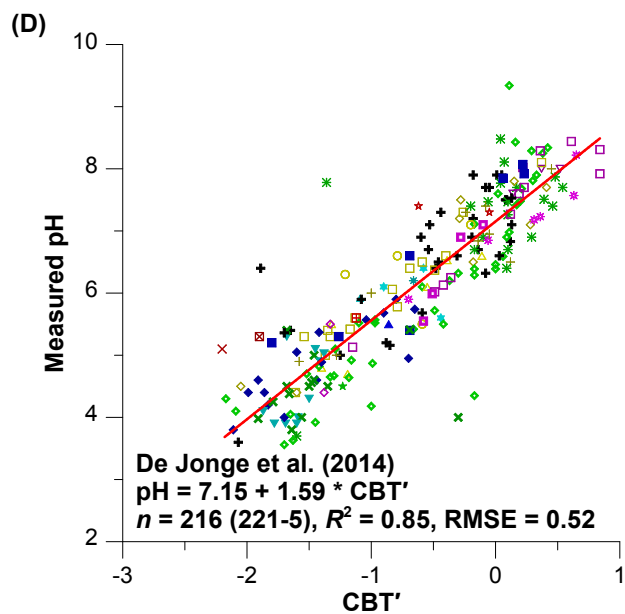
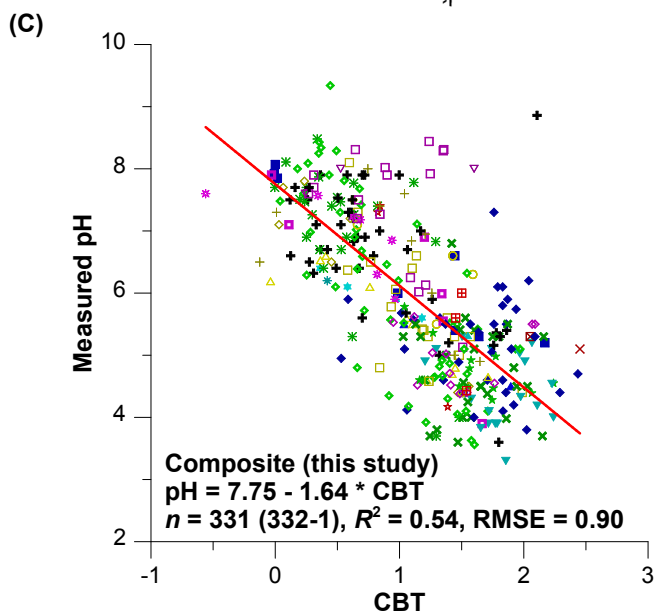
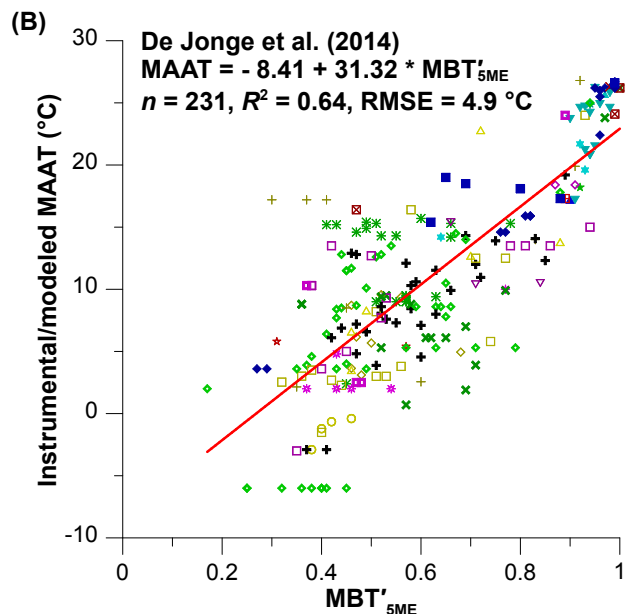
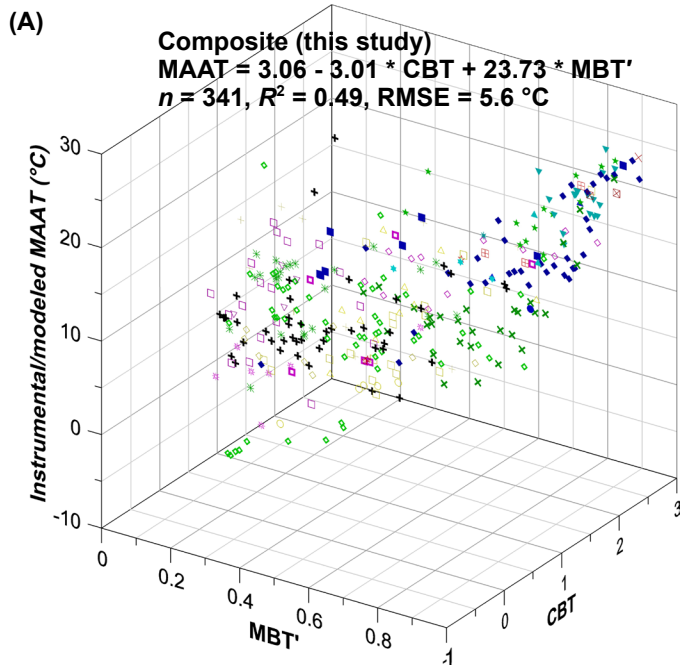
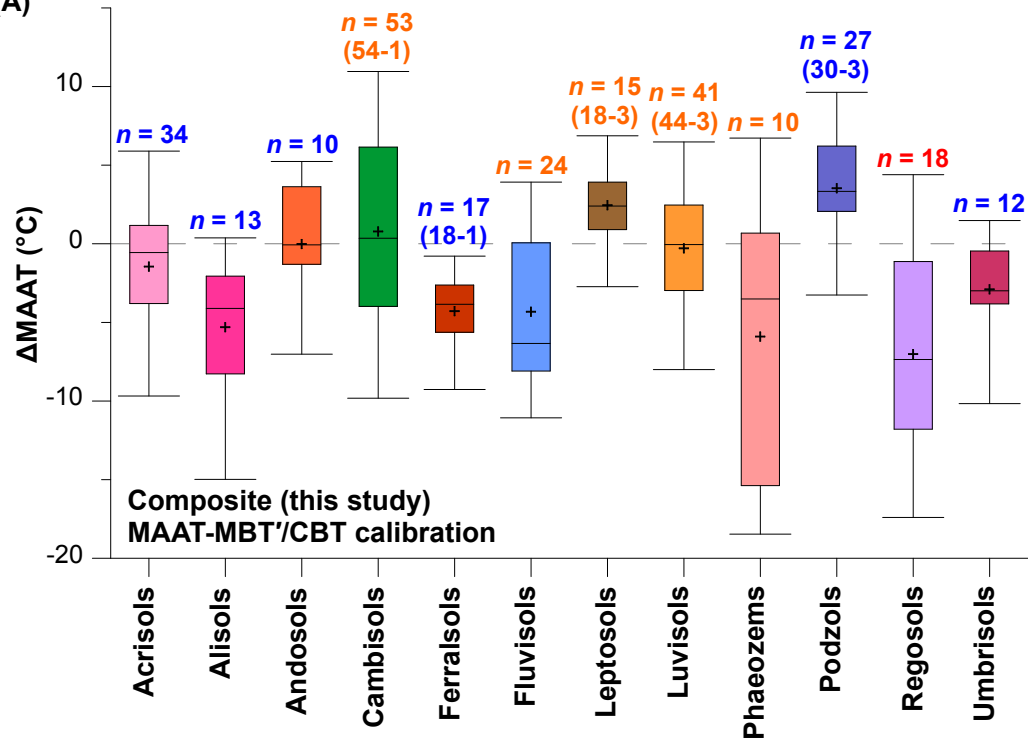
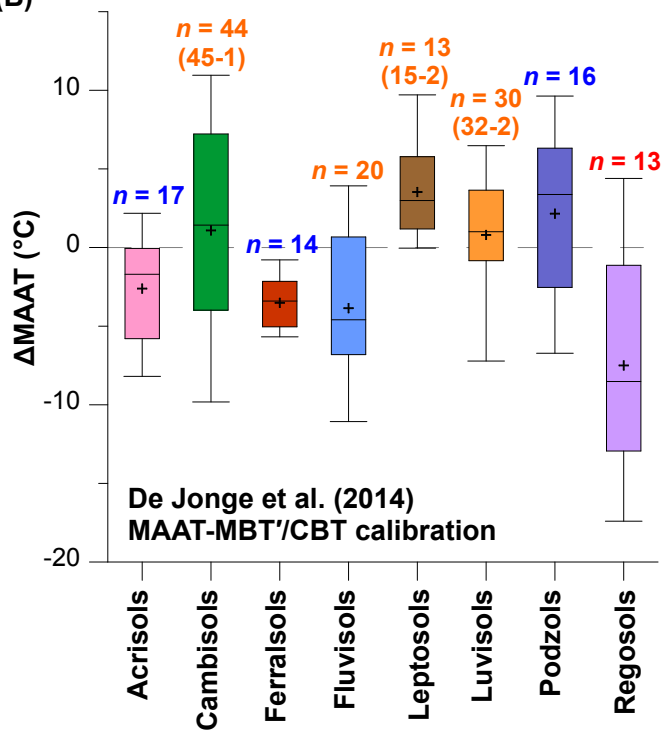


Figure 4 - revised

(A)



(B)



(C)

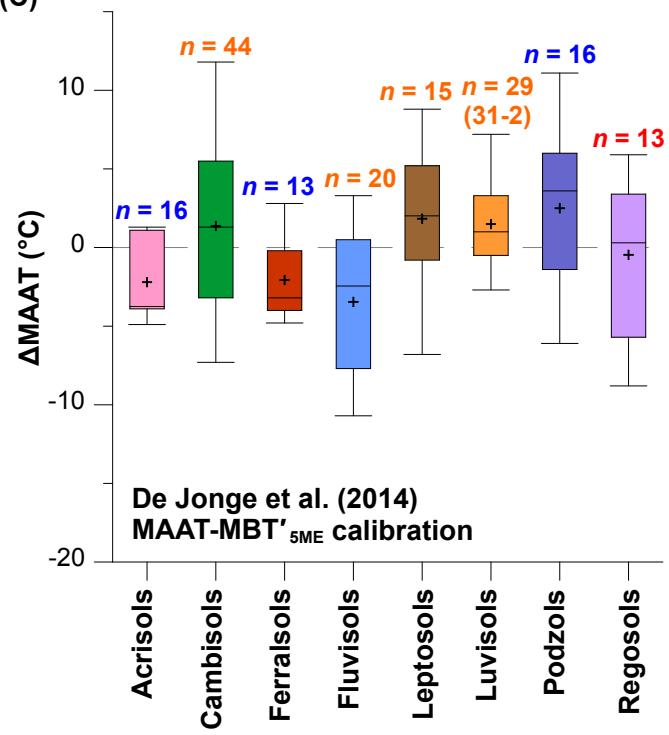


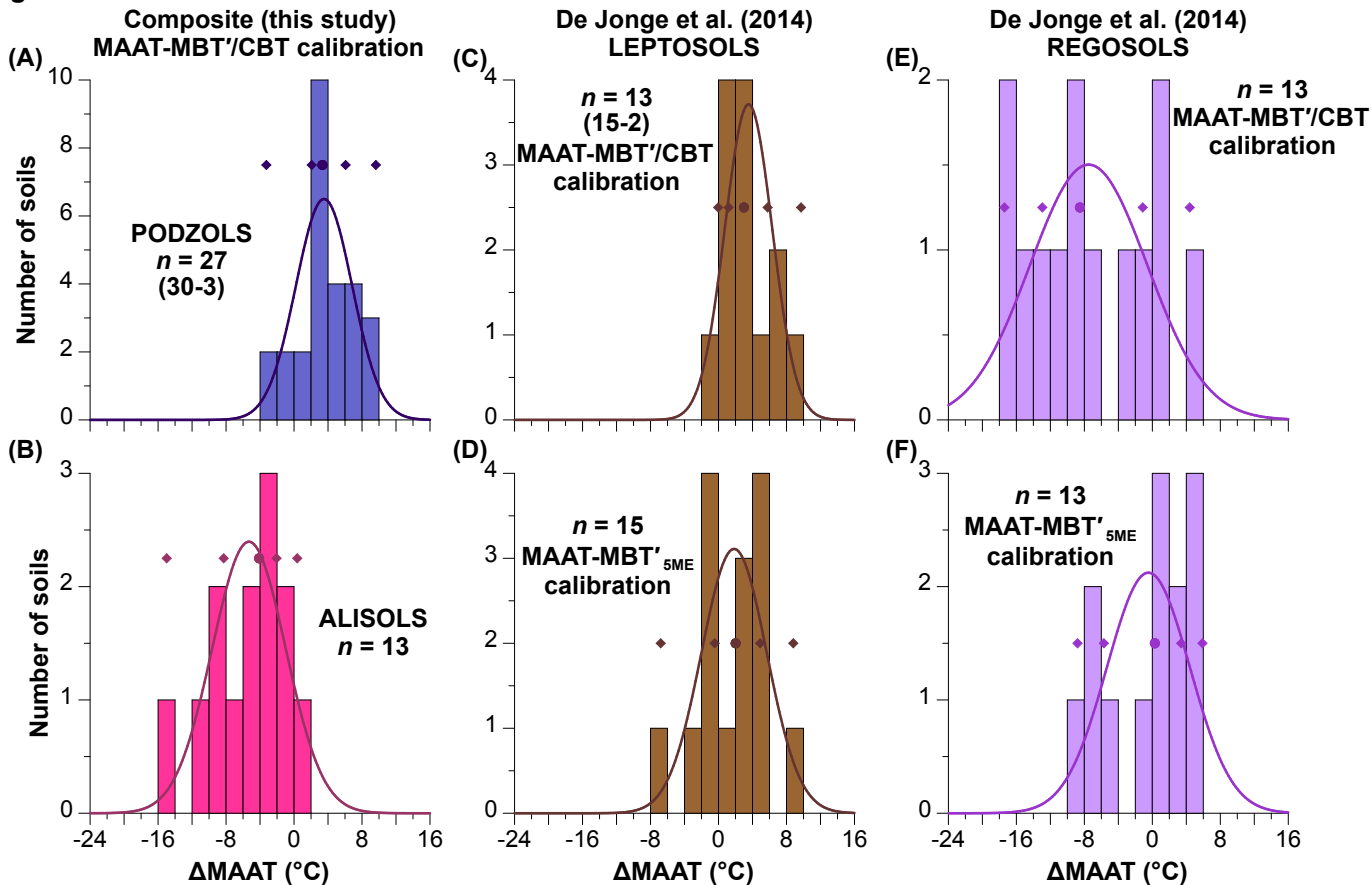
Figure 5 - revised

Figure 6

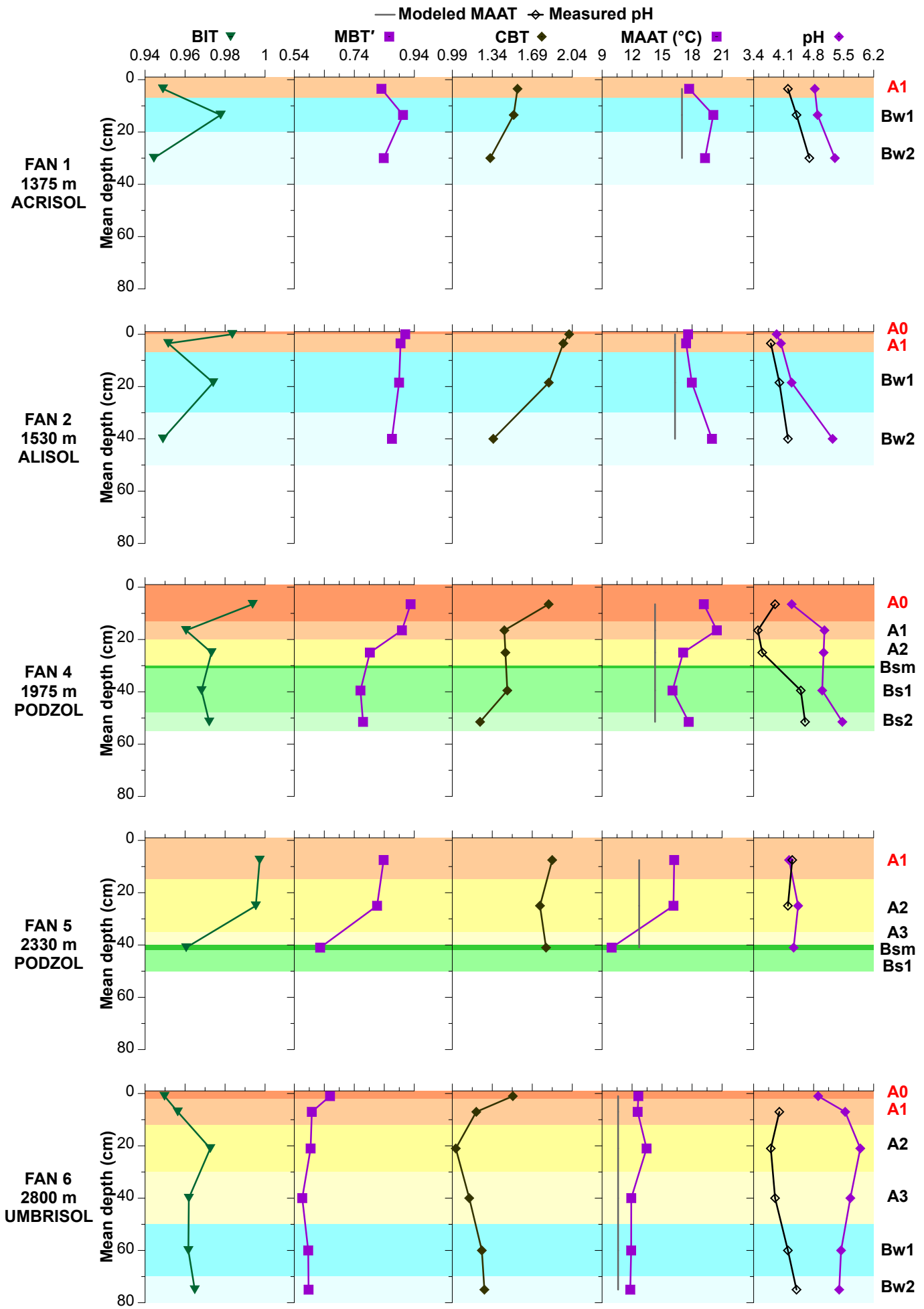


Table 1

	MAAT = a * MBT ^v + b * CBT + c						pH = S * CBT + I						
	<i>n</i>	a	b	c	<i>R</i> ²	<i>p</i>	E	<i>n</i>	S	I	<i>R</i> ²	<i>p</i>	E
All soils	341	23.73 ± 1.43	-3.01 ± 0.65	3.06 ± 0.72	0.5	< 0.001	5.6	331 (332-1)	-1.64 ± 0.08	7.75 ± 0.11	0.5	< 0.001	0.9
Acrisols	33 (34-1)	38.23 ± 3.71	-4.20 ± 1.48	-6.32 ± 2.72	0.8	< 0.001	3.1	33	-0.16 ± 0.32	5.45 ± 0.53	0.0	0.61	0.8
Alisols	13	0.46 ± 5.49	4.49 ± 2.17	15.37 ± 4.17	0.4	0.10	2.3	13	-0.66 ± 0.30	5.79 ± 0.49	0.3	0.052	0.4
Andosols	10	24.61 ± 9.77	-4.22 ± 2.61	2.89 ± 6.10	0.6	0.049	4.4	10	-1.28 ± 0.23	6.74 ± 0.25	0.8	< 0.001	0.4
Cambisols	54	23.64 ± 5.27	-7.20 ± 1.91	4.72 ± 2.18	0.3	< 0.001	6.3	53	-2.32 ± 0.25	8.25 ± 0.27	0.6	< 0.001	0.9
Ferralsols	18	24.07 ± 15.22	-1.90 ± 2.12	5.05 ± 14.80	0.2	0.21	2.5	18	-0.42 ± 0.50	5.19 ± 0.91	0.0	0.41	0.6
Fluvisols	24	5.16 ± 7.84	-0.66 ± 2.72	11.45 ± 2.23	0.0	0.78	3.8	24	-1.91 ± 0.49	8.06 ± 0.33	0.4	0.001	0.9
Leptosols	18	30.55 ± 6.70	-2.19 ± 3.34	-4.63 ± 3.95	0.6	0.001	4.6	18	-1.89 ± 0.44	7.92 ± 0.53	0.5	0.001	0.7
Luvisols	42 (44-2)	15.02 ± 2.78	-4.09 ± 1.02	5.83 ± 1.21	0.5	< 0.001	3.1	40 (41-1)	-1.46 ± 0.22	7.81 ± 0.20	0.5	< 0.001	0.7
Phaeozems	10	4.79 ± 8.88	-7.19 ± 4.19	18.33 ± 6.17	0.4	0.21	7.0	10	-0.95 ± 0.55	7.52 ± 0.59	0.3	0.12	1.0
Podzols	30	23.24 ± 5.53	-2.48 ± 2.98	-1.74 ± 4.75	0.4	0.001	4.3	29	-0.32 ± 0.48	5.27 ± 0.77	0.0	0.51	0.8
Regosols	17 (18-1)	-8.65 ± 8.55	4.27 ± 2.12	7.69 ± 2.35	0.2	0.15	3.4	17	-0.73 ± 0.60	8.07 ± 0.60	0.1	0.25	1.0
Umbrisols	12	15.34 ± 3.92	-0.89 ± 2.15	6.71 ± 3.05	0.7	0.01	2.2	12	0.09 ± 0.43	4.81 ± 0.65	0.0	0.84	0.5

Table 2

		All soils	Acrisols	Cambisols	Ferralsols	Fluvisols	Leptosols	Luvisols	Podzols	Regosols
MAAT = a × MBT' + b × CBT + c	<i>n</i>	234 (235-1)	17	45	14	19 (20-1)	15	30 (32-2)	16	12 (13-1)
	<i>a</i>	27.47 ± 1.79	37.02 ± 2.99	23.61 ± 6.27	37.78 ± 14.23	-10.47 ± 9.61	28.52 ± 8.02	22.14 ± 4.70	24.32 ± 9.20	-22.85 ± 9.57
	<i>b</i>	-4.53 ± 0.78	-2.53 ± 1.23	-7.05 ± 2.29	-3.92 ± 1.69	1.33 ± 2.94	-1.84 ± 3.87	-5.28 ± 1.16	-3.05 ± 6.42	3.81 ± 2.24
	<i>c</i>	2.35 ± 0.88	-6.48 ± 2.33	4.28 ± 2.66	-4.99 ± 14.52	15.77 ± 2.37	-4.34 ± 4.48	3.42 ± 2.02	-1.43 ± 9.82	12.02 ± 2.96
	<i>R</i> ²	0.5	0.9	0.3	0.6	0.1	0.5	0.6	0.4	0.5
	<i>p</i>	< 0.001	< 0.001	0.001	0.003	0.44	0.01	< 0.001	0.053	0.07
	<i>E</i>	5.8	2.3	6.8	1.6	2.9	5.0	3.2	5.9	3.0
MAAT = S × MBT' _{5ME} + I	<i>n</i>	231	16	44	13	20	15	31	16	13
Homogeneity of slopes test: <i>F</i> = 1.59, <i>p</i> = 0.14	<i>S</i>	31.32 ± 1.55	32.96 ± 2.79	31.21 ± 5.31	50.07 ± 28.84	3.91 ± 9.70	31.51 ± 6.27	25.80 ± 4.40	24.41 ± 7.99	15.98 ± 5.75
	<i>I</i>	-8.41 ± 1.01	-7.65 ± 2.40	-9.74 ± 2.80	-24.01 ± 27.14	10.17 ± 5.39	-10.36 ± 3.57	-6.18 ± 2.62	-6.59 ± 5.25	0.61 ± 3.43
ANCOVA: <i>F</i> = 5.34, <i>p</i> < 0.001	<i>R</i> ²	0.6	0.9	0.5	0.2	0.0	0.7	0.5	0.4	0.4
	<i>p</i>	< 0.001	< 0.001	< 0.001	0.11	0.69	< 0.001	< 0.001	0.01	0.02
	<i>E</i>	4.9	2.5	5.6	2.4	3.7	4.1	3.2	5.5	4.1
pH = S × CBT + I	<i>n</i>	231 (232-1)	16	44	14	20	15	31 (32-1)	16	13
	<i>S</i>	-1.75 ± 0.10	-0.63 ± 0.27	-2.44 ± 0.29	-0.56 ± 0.63	-2.20 ± 0.51	-2.11 ± 0.36	-1.55 ± 0.23	-0.54 ± 0.50	-0.77 ± 0.80
Homogeneity of slopes test: <i>F</i> = 3.83, <i>p</i> = 0.001	<i>I</i>	7.90 ± 0.12	5.86 ± 0.44	8.35 ± 0.31	5.47 ± 1.12	8.18 ± 0.32	8.31 ± 0.42	7.84 ± 0.22	5.32 ± 0.83	8.11 ± 0.86
	<i>R</i> ²	0.6	0.3	0.6	0.1	0.5	0.7	0.6	0.1	0.1
	<i>p</i>	< 0.001	0.03	< 0.001	0.39	< 0.001	< 0.001	< 0.001	0.30	0.36
	<i>E</i>	0.9	0.6	0.9	0.7	0.9	0.5	0.7	0.5	1.1
pH = S × CBT' + I	<i>n</i>	216 (221-5)	15	42 (44-2)	10	17 (19-2)	15	31	14	12
	<i>S</i>	1.59 ± 0.05	1.14 ± 0.20	1.78 ± 0.10	1.97 ± 1.03	0.56 ± 0.61	1.66 ± 0.11	1.29 ± 0.18	0.18 ± 0.33	1.76 ± 0.19
Homogeneity of slopes test: <i>F</i> = 4.64, <i>p</i> < 0.001	<i>I</i>	7.15 ± 0.05	6.49 ± 0.30	7.04 ± 0.10	7.59 ± 1.65	7.32 ± 0.16	7.43 ± 0.12	7.25 ± 0.14	4.75 ± 0.49	7.11 ± 0.11
	<i>R</i> ²	0.8	0.7	0.9	0.3	0.1	0.9	0.6	0.0	0.9
	<i>p</i>	< 0.001	< 0.001	< 0.001	0.09	0.37	< 0.001	< 0.001	0.59	< 0.001
	<i>E</i>	0.5	0.4	0.5	0.5	0.5	0.2	0.6	0.5	0.4

Table 3

Sample	Altitude (m)	Coordinates	Horizon	Mean depth (cm)	C _{org} (%)	H ₂ O (%)	Measured pH	Modeled MAAT (°C)	BIT	MBT'	CBT	Calculated MAAT (°C)	Calculated pH
FAN1.1	1375	22°19'15"N 103°49'52"E	A1	3.5	8.27	76	4.2	17.0	0.95	0.83	1.56	17.7	4.8
FAN1.2			Bw1	13.5	2.72	nd	4.4		0.98	0.90	1.53	20.1	4.9
FAN1.3			Bw2	30	0.62	60	4.7		0.94	0.84	1.32	19.3	5.3
FAN2.A0	1530	22°18'44"N 103°49'25"E	A0	0	nd	nd	nd	16.3	0.98	0.91	2.01	17.6	3.9
FAN2.1			A1	3.5	4.30	80	3.8		0.95	0.89	1.96	17.4	4.0
FAN2.2			Bw1	18.5	2.54	nd	4.0		0.97	0.89	1.83	18.0	4.3
FAN2.3			Bw2	40	0.66	50	4.2		0.95	0.87	1.35	20.0	5.2
FAN4.1	1975	22°18'20"N 103°48'38"E	A0	6.5	44.13	nd	3.9	14.3	0.99	0.93	1.83	19.2	4.3
FAN4.2			A1	16.5	8.11	215	3.5		0.96	0.90	1.45	20.5	5.1
FAN4.3			A2	25	3.59	66	3.6		0.97	0.79	1.46	17.1	5.0
FAN4.5			Bs1	39.5	1.22	40	4.5		0.97	0.76	1.47	16.0	5.0
FAN4.6			Bs2	51.5	1.16	nd	4.6		0.97	0.77	1.23	17.7	5.5
FAN5.1			2330	22°18'00"N 103°48'36"E	A1	7.5	5.99		114	4.3	12.7	1.00	0.84
FAN5.2	A2	25			4.38	nd	4.2	1.00	0.82	1.76		16.1	4.4
FAN5.4	Bsm	41			nd	nd	nd	0.96	0.63	1.81		10.0	4.3
FAN6.1	2800	22°17'32"N 103°48'02"E	A0	1	6.14	nd	nd	10.6	0.95	0.66	1.52	12.6	4.9
FAN6.2			A1	7	3.89	106	4.0		0.96	0.60	1.20	12.6	5.5
FAN6.3			A2	21	2.95	nd	3.8		0.97	0.59	1.02	13.5	5.9
FAN6.4			A3	40	2.07	53	3.9		0.96	0.57	1.14	11.9	5.7
FAN6.5			Bw1	60	0.77	nd	4.2		0.96	0.59	1.25	11.9	5.4
FAN6.6			Bw2	75	0.39	nd	4.4		0.96	0.59	1.27	11.8	5.4